



Article

# Synthesis and Characterization of Tetraphenylethene AIEgen-Based Push–Pull Chromophores for Photothermal Applications: Could the Cycloaddition–Retroelectrocyclization Click Reaction Make Any Molecule Photothermally Active?

Maxime Roger<sup>1</sup>, Yann Bretonnière<sup>2</sup>, Yann Trolez<sup>3</sup> , Antoine Vacher<sup>3</sup>, Imane Arbouch<sup>4</sup> , Jérôme Cornil<sup>4</sup>, Gautier Félix<sup>1</sup> , Julien De Winter<sup>5</sup> , Sébastien Richeter<sup>1</sup>, Sébastien Clément<sup>1,\*</sup> and Philippe Gerbier<sup>1,\*</sup>

<sup>1</sup> ICGM, CNRS UMR 5253, ENSCM, University of Montpellier, 34293 Montpellier, France; maxime.roger@univ-angers.fr (M.R.); gautier.felix@umontpellier.fr (G.F.); sebastien.richeter@umontpellier.fr (S.R.)

<sup>2</sup> ENS de Lyon, CNRS UMR 5182, Laboratoire de Chimie, University of Lyon, 69364 Lyon, France; yann.bretonniere@ens-lyon.fr

<sup>3</sup> Ecole Nationale Supérieure de Chimie de Rennes, CNRS, ISCR—UMR 6226, University of Rennes, 35065 Rennes, France; yann.trolez@ensc-rennes.fr (Y.T.); antoine.vacher@univ-rennes1.fr (A.V.)

<sup>4</sup> Laboratory for Chemistry of Novel Materials, University of Mons-UMONS, 7000 Mons, Belgium; imane.arbouch@umons.ac.be (I.A.); jerome.cornil@umons.ac.be (J.C.)

<sup>5</sup> Organic Synthesis and Mass Spectrometry Laboratory (S2MOs), University of Mons-UMONS, 7000 Mons, Belgium; julien.dewinter@umons.ac.be

\* Correspondence: sebastien.clement1@umontpellier.fr (S.C.); philippe.gerbier@umontpellier.fr (P.G.)



**Citation:** Roger, M.; Bretonnière, Y.; Trolez, Y.; Vacher, A.; Arbouch, I.; Cornil, J.; Félix, G.; De Winter, J.; Richeter, S.; Clément, S.; et al. Synthesis and Characterization of Tetraphenylethene AIEgen-Based Push–Pull Chromophores for Photothermal Applications: Could the Cycloaddition–Retroelectrocyclization Click Reaction Make Any Molecule Photothermally Active? *Int. J. Mol. Sci.* **2023**, *24*, 8715. <https://doi.org/10.3390/ijms24108715>

Academic Editor: Andrea Pace

Received: 13 April 2023

Revised: 4 May 2023

Accepted: 10 May 2023

Published: 13 May 2023



**Copyright:** © 2023 by the authors. Licensee MDPI, Basel, Switzerland. This article is an open access article distributed under the terms and conditions of the Creative Commons Attribution (CC BY) license (<https://creativecommons.org/licenses/by/4.0/>).

**Abstract:** Three new tetraphenylethene (TPE) push–pull chromophores exhibiting strong intramolecular charge transfer (ICT) are described. They were obtained via [2 + 2] cycloaddition–retroelectrocyclization (CA-RE) click reactions on an electron-rich alkyne-tetrafunctionalized TPE (TPE-alkyne) using both 1,1,2,2-tetracyanoethene (TCNE), 7,7,8,8-tetracyanoquinodimethane (TCNQ) and 2,3,5,6-tetrafluoro-7,7,8,8-tetracyanoquinodimethane (F<sub>4</sub>-TCNQ) as electron-deficient alkenes. Only the starting TPE-alkyne displayed significant AIE behavior, whereas for TPE-TCNE, a faint effect was observed, and for TPE-TCNQ and TPE-F<sub>4</sub>-TCNQ, no fluorescence was observed in any conditions. The main ICT bands that dominate the UV–Visible absorption spectra underwent a pronounced red-shift beyond the near-infrared (NIR) region for TPE-F<sub>4</sub>-TCNQ. Based on TD-DFT calculations, it was shown that the ICT character shown by the compounds exclusively originated from the clicked moieties independently of the nature of the central molecular platform. Photothermal (PT) studies conducted on both TPE-TCNQ and TPE-F<sub>4</sub>-TCNQ in the solid state revealed excellent properties, especially for TPE-F<sub>4</sub>-TCNQ. These results indicated that CA-RE reaction of TCNQ or F<sub>4</sub>-TCNQ with donor-substituted are promising candidates for PT applications.

**Keywords:** TPE; AIEgen; cycloaddition-retroelectrocyclization; click chemistry; photothermal applications

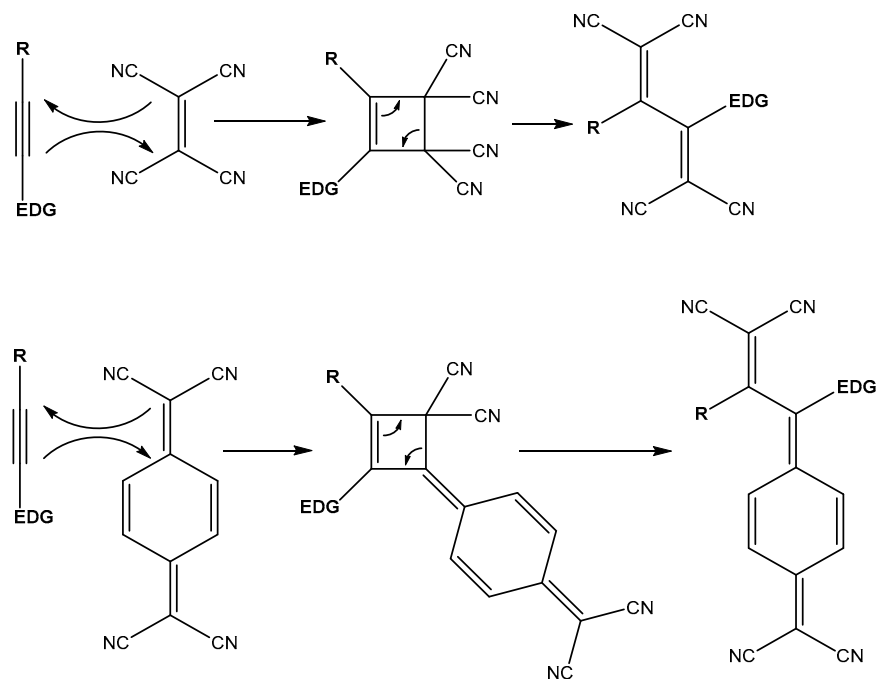
## 1. Introduction

Although the phenomenon has been known and briefly described before [1], it was Ben Zhong Tang who first described and tried to explain the unusual behavior of 1-methyl-1,2,3,4,5-pentaphenylsilole, which was not luminescent in solution in a good solvent but became highly emissive in the solid state [2]. This very rare behavior, called Aggregation-Induced Emission (AIE), is opposed to the behavior classically encountered in fluorophores with a planar and rigid structure, which are generally fluorescent in solution and non-emissive in the solid state (Aggregation-Caused Quenching—ACQ). Following this work, in just over 20 years, the number of publications concerning the description of new AIE luminogens (AIEgens) has increased exponentially [3], and the mechanisms leading to the observation of this phenomenon are now well known [4–6]. The considerable success

of the AIE phenomenon lies in the fact that it makes possible it to effectively address a major issue, which is the emission in the solid or aggregated state of molecules, a problem of the utmost importance for many scientific fields or technological applications [4,7,8]. Among the many areas taking advantage of AIEgens, we can mention optoelectronics with OLEDs [9,10], stimuli-responsive materials [11–13], anticounterfeiting or encryption [12,14], sensing [15–17] and biology or medicine, fields in which the use of AIEgens has enabled spectacular advances [18–23]. Indeed, AIEs are used in the fields of imaging [24,25], elucidation of biological processes [26–28], innovative therapies such as photodynamic therapy (PDT) [29–31], photothermal therapy (PTT) [32,33], sonodynamic therapy enhancement [34], cocktail therapy [35] and theranostics [36,37]. Due to the specificity of biological applications, it is necessary to trigger the AIEgens with light in the near-infrared (NIR) domain, which has the advantage on the one hand of not being harmful to the cells, and on the other hand of having a good depth of penetration into the living tissues [38,39]. As a result, it was necessary to substantially reduce the HOMO–LUMO energy gap ( $E_g$ ) of conventional AIEgens whose absorption bands are located in the UV range. Different strategies can be considered to increase the excitation and emission wavelengths of the fluorophores. The first one consists of increasing the conjugation length of the  $\pi$ -system. However, this strategy is rapidly discarded due to solubility issues, which require “decorating” the molecules with flexible chains. The second one consists of introducing electron-attracting (A) and/or donating (D) groups into the  $\pi$ -conjugated system [40–42]. Such groups induce changes in orbital energy levels, either an increase in HOMO energy level (influence of donor group), or a decrease in LUMO energy level (influence of attracting group) of the molecule leading to a narrowing of the  $E_g$  [43]. Among the attractor groups yielding the best results are the dicyanovinyl groups. For instance, the latter can be introduced via a Knoevenagel condensation reaction of malonitrile on an AIEgen functionalized with a carbonyl [39,44]. Another approach consists of taking advantage of the “click-chemistry” introduced by K. B. Sharpless, which is effective in introducing various groups under mild, catalyst-free and atom-saving conditions [45]. More especially, the [2 + 2] cycloaddition–retroelectrocyclizations (CA-RE) that involve the reaction between an electron-rich alkyne and an electron-deficient alkene (Scheme 1) have recently attracted significant attention [46,47]. The CA-RE reaction was first reported by M. I. Bruce in 1981 in the field of organometallic chemistry by reacting 1,1,2,2-tetracyanoethene (TCNE) with metallocene-substituted acetylides [48]. It was 18 years later that it was used for the synthesis of DA-type thiophenevinylidene derivatives for nonlinear optical (NLO) applications in the groups of A. K.-Y. Jen and U. W. Suter [49,50]. This reaction has been widely exploited and studied by the group of F. Diederich to develop a new platform of simple molecules with nonlinear optical (NLO) properties [51,52]. In the continuation of these works, he showed that it was possible to modulate the optical and electrochemical properties of the clicked compounds by extending the CA-RE reaction to other electron-deficient alkenes which have a similar reactivity, such as 7,7,8,8-tetracyanoquinodimethane (TCNQ) and 2,3,5,6-tetrafluoro-7,7,8,8-tetracyanoquinodimethane ( $F_4$ -TCNQ) [53–55]. Since then, researchers have used CA-RE to synthesize D- $\pi$ -A push–pull systems to be used in various applications such as optoelectronics [56–68], NLO [69–71], photoacoustic (PA) imaging [72–76] and theranostics [77]. Surprisingly, although the photoacoustic and photothermal (PT) phenomena are related, very few papers describe the use of CA-RE clicked products for PT applications [72,78].

In this work, we used the [2 + 2] CA-RE reaction with the aim of obtaining new AIE-based PT materials displaying a strong charge transfer character. We chose the AIEgen archetypal tetraphenylethene (TPE) as the central core due to its very good ability to retain its AIE properties, although it is incorporated in more complicated molecular architectures [79,80]. Moreover, when linked to naphthalene diimide-fused 2-(1,3-dithiol-2-ylidene)acetonitrile derivatives, it has already shown its ability to lead to AIE-based PT materials [81]. In order to achieve the CA-RE reactions, we functionalized the four arms of the TPE with  $C\equiv C$  triple bonds capped by dialkylanilino moieties as electron-donor groups.

The resulting clicked products with TCNE, TCNQ and F<sub>4</sub>-TCNQ showed a pronounced CT characterized by an NIR strong absorption, in particular, for TPE-TCNQ and TPE-F<sub>4</sub>-TCNQ, in the biological transparency window (NIR-I, 750–1000 nm). These two latter products were found to possess good thermal properties, allowing them to display rather good photothermal performances.



**Scheme 1.** Mechanism of the CA-RE click reaction between TCNE (**top**) or TCNQ (**bottom**) and alkynes activated by an electron-donor group (EDG). When TCNQ is used, the quinoidal moiety is located next to the EDG group [54,82].

## 2. Results and Discussion

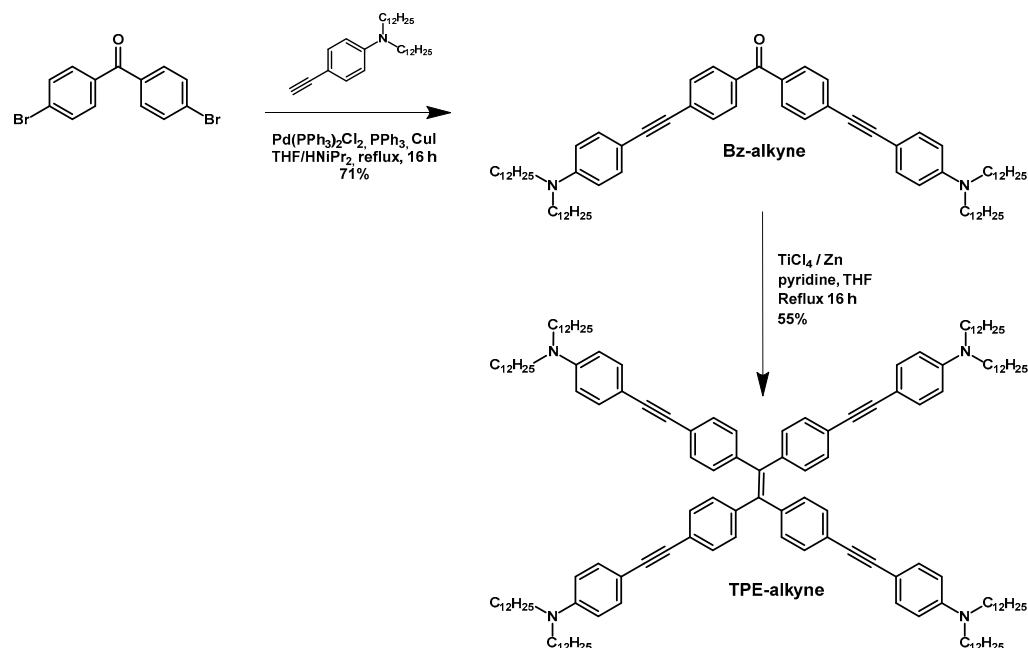
### 2.1. Synthesis

The preparation of compounds TPE-TCNE, TPE-TCNQ and TPE-F<sub>4</sub>-TCNQ started with TPE-alkyne, whose synthesis involved a McMurry homocoupling reaction of the benzophenone derivative Bz-alkyne with a yield of 55% (Scheme 2). Bz-alkyne was synthesized in 71% yield by using a Sonogashira cross-coupling reaction between 4,4'-dibromobenzophenone and *N,N'*-didodecyl-4-ethynylaniline. All attempts to obtain TPE-alkyne through a Sonogashira cross-coupling reaction between 1,1,2,2-tetrakis(4-bromophenyl)ethene and *N,N'*-didodecyl-4-ethynylaniline invariably conducted to inseparable mixtures of diversely substituted compounds.

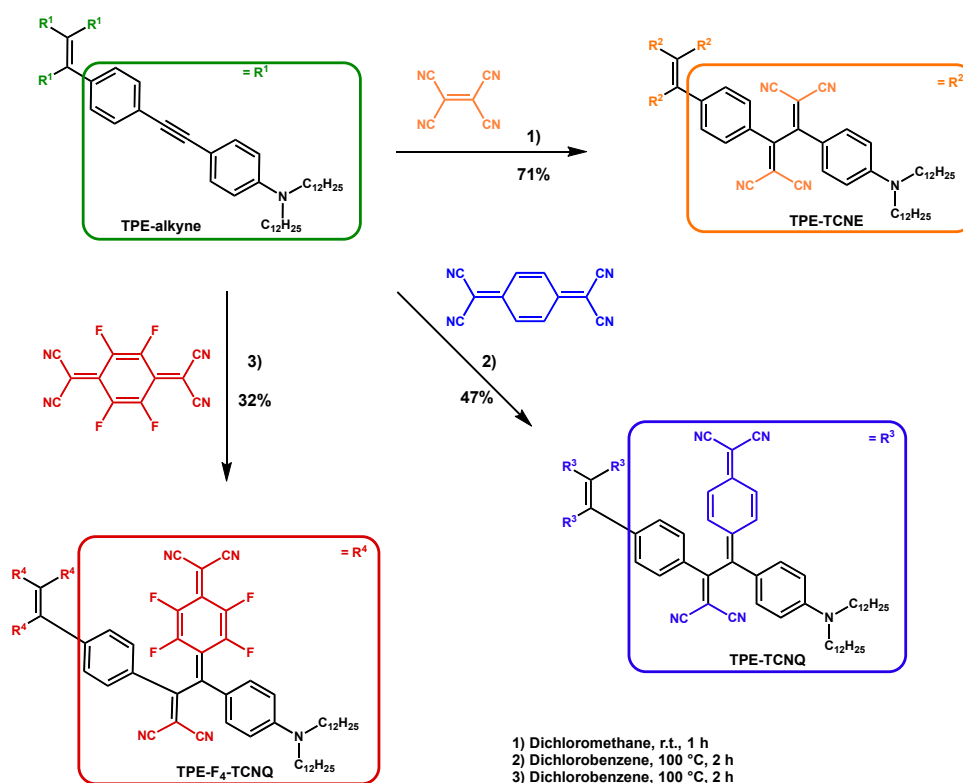
Finally, [2 + 2] CA-RE reactions were conducted by using a 50% excess of tetracyano derivatives (TCNE, TCNQ and F<sub>4</sub>-TCNQ) in various solvents at room temperature to form TPE-TCNE, TPE-TCNQ and TPE-F<sub>4</sub>-TCNQ as dark film-forming solids after purification with column chromatography on silica gel (Scheme 3).

All the compounds were fully characterized by <sup>1</sup>H, <sup>13</sup>C{<sup>1</sup>H}, <sup>19</sup>F{<sup>1</sup>H} NMR spectroscopy and high-resolution mass spectrometry (HR-MS) (see ESI for spectral details). Examining their <sup>1</sup>H NMR spectra, some interesting points can be noted (Figure 1): (i) as expected, the grafting of electron-withdrawing groups on the triple bond led to a deshielding of the protons located in their vicinity (doublets in the aromatic region), as well as those of the methylene groups bonded to the nitrogen atoms of the aniline moieties ( $\delta = 3.25 - 3.55$  ppm); (ii) the comparison of the chemical shifts of the aromatic protons between TPE-alkyne, TPE-TCNE and TPE-TCNQ highlighted the localization of the dicyanoquinomethanyl moiety on the aniline side in agreement with previous findings [54]; (iii) due to the highly twisted conformation of the butadiene in TPE-TCNQ (see ESI), all

the protons present in the quinoid ring are not equivalents, giving rise to four doublets among which two are clearly seen in Figure 1 (see ESI for more details) and *iv*) the spectrum obtained for TPE-F<sub>4</sub>-TCNQ is poorly resolved, implying the presence of paramagnetic species as observed elsewhere [46,53]. Indeed, the ESR spectrum of a THF solution of TPE-F<sub>4</sub>-TCNQ showed an unresolved weak signal with a *g* factor of 2.0027 and a band width of 7.50 G, whereas, in the solid state, a much more intense signal with a *g* factor of 2.0021 and a band width of 10.25 G was observed (Figure 2).



Scheme 2. Reaction pathway towards TPE-alkyne.



Scheme 3. Synthetic scheme of compounds TPE-alkyne, TPE-TCNQ and TPE-F<sub>4</sub>-TCNQ.

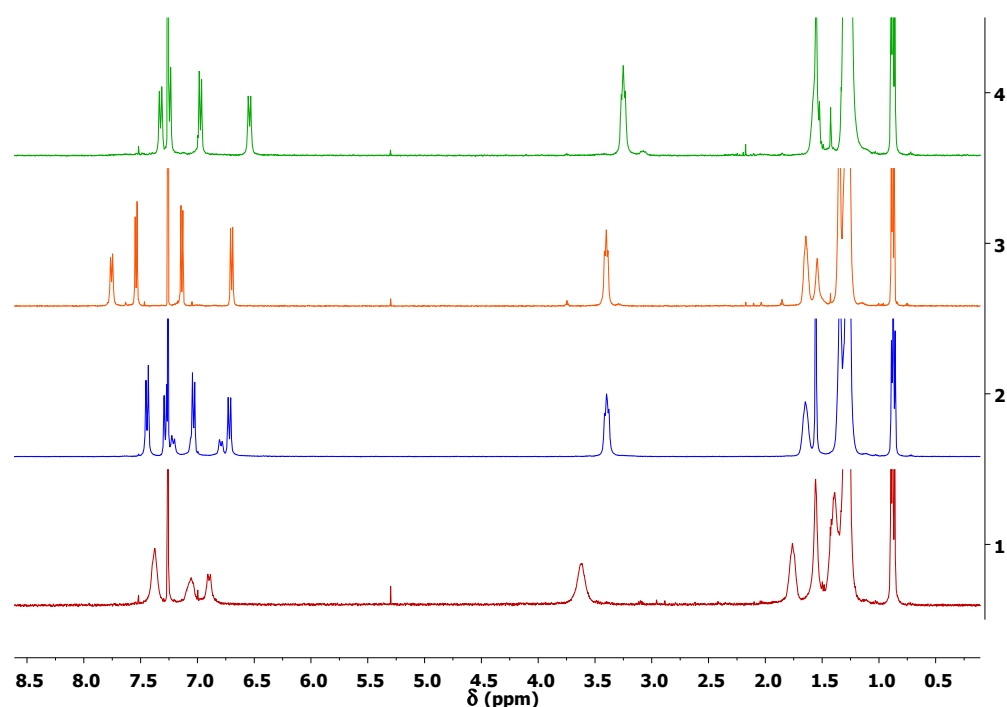


**Figure 1.**  $^1\text{H}$  NMR spectra of TPE-alkyne (green), TPE-TCNE (orange), TPE-TCNQ (blue) and TPE- $\text{F}_4$ -TCNQ (red) recorded in  $\text{CDCl}_3$ .

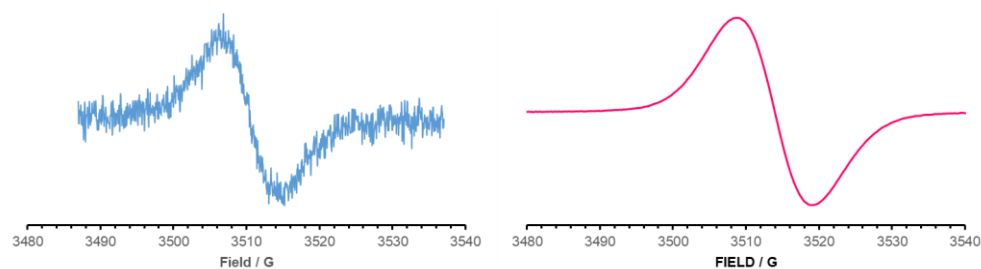


**Figure 2.** ESR spectra of TPE- $\text{F}_4$ -TCNQ in THF solution (right) and in the solid state (left), recorded at room temperature.

## 2.2. Photophysical Properties

The UV–Visible absorption spectra of the investigated compounds are shown in Figure 3. The starting compound TPE-alkyne only showed a major absorption peak at 359 nm corresponding to a  $\pi$ - $\pi^*$  transition (vide supra). Contrastingly, the spectra of TPE-TCNE, TPE-TCNQ and TPE- $\text{F}_4$ -TCNQ showed additional intense absorption peaks in the visible–NIR region (see Table 1 for data). These peaks possessed strong molar extinction coefficients, likely corresponding to intramolecular charge transfer (ICT) absorptions involving the terminal amino groups and dicyanovinyl moieties [76]. Moreover, as observed previously, the effect of the increasing electron-withdrawing strength of the adduct that is  $\text{F}_4$ -TCNQ > TCNQ > TCNE is witnessed by a marked bathochromic shift in the CT absorption [70–72,83–86]. Besides the intense charge transfer band involving the dicyanoquinoid moieties (CT band B) observed above 600 nm for TPE-TCNQ and TPE- $\text{F}_4$ -TCNQ, the less intense CT band (CT band A) that was observed for all the clicked compounds in the 450–550 nm region involved the dicyanovinyl moieties (see Figure 4) [76]. Finally, although this is commonly observed for compounds exhibiting a charge transfer phenomenon, we have not demonstrated solvatochromism for these TPE adducts [66]. This may be related to the symmetry of these molecules, which implies that they have a weak total dipolar moment in the excited state. The absorbance spectra of all adducts deposited as thin films on quartz slides were like those recorded in THF solutions (Figure S23). As

seen in Table 1, the longer wavelength absorptions experienced moderate (TPE-TCNE: 7 nm and TPE-4F-TCNQ: 15 nm) to appreciable (TPE-TCNQ: 50 nm) red shifts in the solid state.

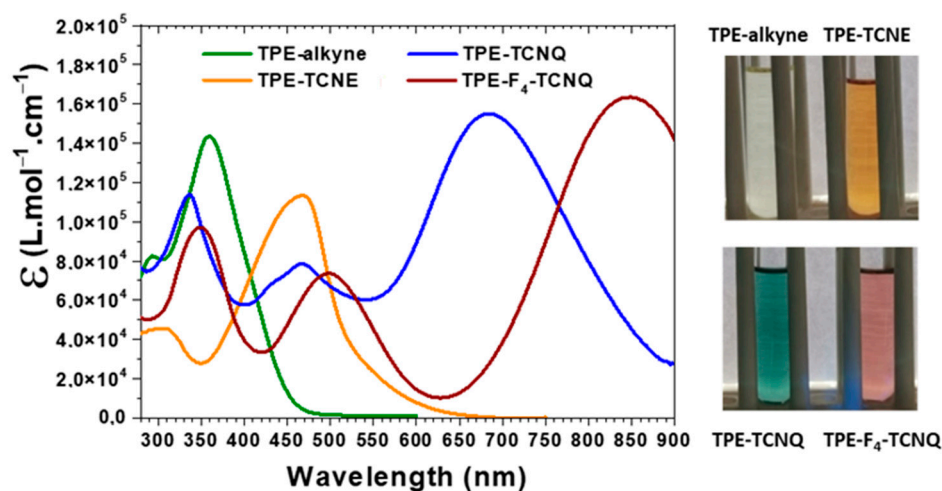


**Figure 3.** UV-Visible absorption spectra of investigated compounds in THF solutions ( $C = 6 \times 10^{-6}$  M) (left) and images of their corresponding solutions (right).

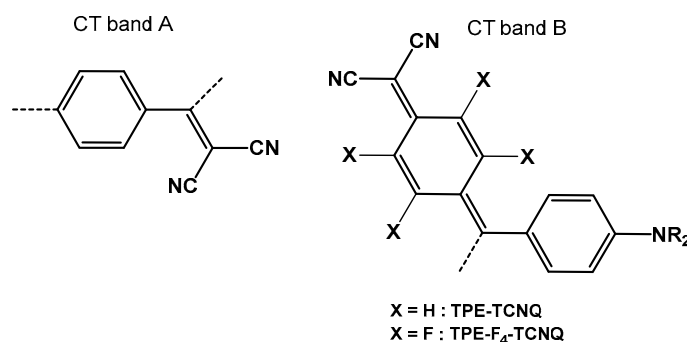


**Figure 4.** Chromophores likely involved in the CT bands A and B.

**Table 1.** Optical data (absorbance and fluorescence) for the investigated compounds recorded in solution or in the aggregated state.

	TPE-Alkyne	TPE-TCNE	TPE-TCNQ	TPE-F <sub>4</sub> -TCNQ
Absorbance in solution <sup>a</sup> (nm)/( $\epsilon$ (L·mol <sup>-1</sup> ·cm <sup>-1</sup> ))	294 (82,400) 359 (143,400)	307/(45,600) 469 (113,400)	337 (113,900) 468 (78,500) 688 (155,000)	348 (97,500) 497 (73,600) 849 (163,400)
Absorbance as thin films (nm)	-	476	471; 738	498; 864
$\lambda_{em\ max}$ (solution <sup>a</sup> /aggregated <sup>b</sup> )	582/560/-	$\approx$ 700/786	-	-
$\Phi_{sol}$ (%) <sup>a</sup>	13%	-	-	-
$\Phi_{aggr}$ (%) <sup>b</sup>	21%	ND	-	-
$\lambda_{onset}$ (nm) <sup>c</sup>	460	540	900	-
$E_{g\ opt}$ (eV) <sup>d</sup>	2.70	2.30	1.38	-

<sup>a</sup> measured in THF, <sup>b</sup> 10% THF/90% H<sub>2</sub>O, <sup>c</sup> Estimated from the extrapolation of the absorption curve of TPE-TCNQ, <sup>d</sup> Calculated using the relation  $E = 1.6 \times 10^{-19}$  (h.c./ $\lambda_{onset}$ ). ND: not determined (see Characterization Methods part).

The fluorescence spectra were also recorded both in solution (THF) and in the aggregated state for all compounds. As observed in most cases with CA-RE products [87–89], only the TPE-alkyne precursor exhibited appreciable fluorescence with an emission maximum at 582 nm and a quantum yield of 13%. A faint fluorescence was detected for TPE-TCNE with an emission maximum at ca. 700 nm and a quantum yield lower than 1%. The corresponding spectra are shown in Figure 5. Interestingly, the emission maximum showed a dependence on the pH of the solution with a red-shift of 44 nm in acidic medium (see Figure S26). As observed with most TPE derivatives, the emission intensity increased markedly when going from the solution to the aggregated state, indicating an AIE behavior [79]. Consequently, we decided to follow the evolution of the emission spectra of both TPE-alkyne and TPE-TCNE in various mixtures of THF/water, water being a bad solvent for these compounds that should induce an aggregation phenomenon at a certain percentage. As shown in Figure 6, the emission intensity gradually increased as the water percentage exceeded 20% for TPE-alkyne, and more abruptly above 70% for TPE-TCNE, indicating that the presence of the dicyanovinyl moieties induced an increase in water solubility. Interestingly, both compounds exhibited an opposite shift when passing from the solvated to the aggregated state, with TPE-alkyne experiencing a slight blue-shift, whereas for TPE-TCNE, a more pronounced red-shift was noticed.

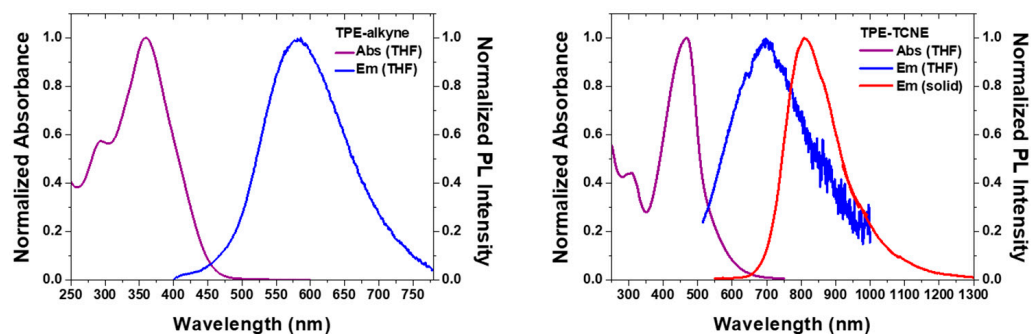


**Figure 5.** UV-Visible absorption and fluorescence spectra of TPE-alkyne (left) and TPE-TCNE (right) recorded in solution and in the solid state.

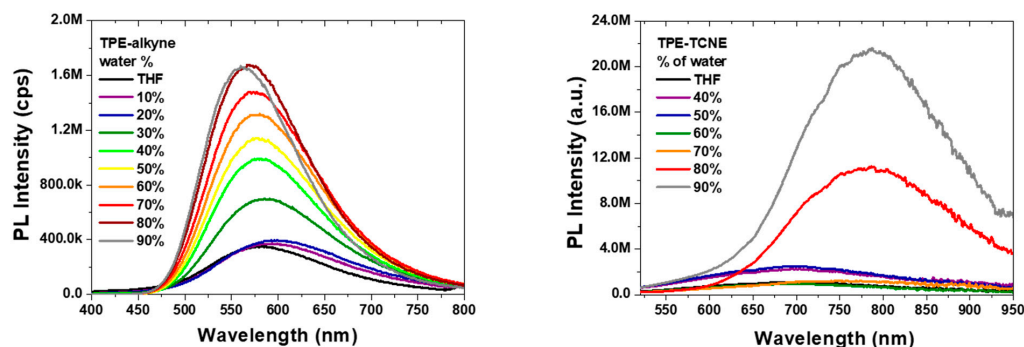


**Figure 6.** Evolution of the emission spectra as a function of water content in THF solutions for TPE-alkyne (left) and TPE-TCNE (right, the emission spectra recorded with 20 and 30% of water are strictly the same as those recorded at 0 and 40%).

### 2.3. Electrochemistry

To evaluate the electronic properties of the different cycloadducts, their cyclic voltammograms (CVs) were recorded as along with the CV of the TPE-alkyne precursor for comparison (see Figure 7). This latter only showed one irreversible oxidation wave at around 0.80 V vs. SCE (peak potential), which could be attributed to the oxidation of the four anilines. One can notice that the four oxidations occurred at the same potential, probably because of the low conjugation between anilines due to the twisted geometry around the central TPE core. This irreversible oxidation was also observed in the case of

cycloadducts, but it was shifted to higher potentials (peak potentials at 1.31 V vs. SCE for TPE-TCNE, 0.88 V vs. SCE for TPE-TCNQ and 0.97 V vs. SCE for TPE-F<sub>4</sub>-TCNQ). This may be attributed to the presence of the strong electron acceptors conjugated to the anilines, rendering their oxidations more difficult. By contrast with the TPE-alkyne precursor, two reversible reduction waves were also observed. The reduction potentials strongly depend on the nature of the electron-accepting groups. In the case of TPE-TCNE, the two reductions occurred at  $-0.45$  and  $-0.88$  V vs. SCE (these potentials were calculated as the half-sum of the anodic and cathodic potential peaks, see the note in Table 2), which are in line with previously reported values for this kind of tetracyanobutadiene (TCBD) [52]. TPE-TCNQ was easier to reduce with reductions at  $-0.23$  and  $-0.46$  V vs. SCE due to a higher delocalization of the newly formed negative charges thanks to the dicyanoquinodimethane moiety. The reduction potentials were even higher in the case of TPE-F<sub>4</sub>-TCNQ:  $+0.09$  and  $-0.21$  V vs. SCE due to the significant strengthening of the electron-accepting ability of the dicyanoquinodimethane moiety due to the presence of the fluorine atoms [54]. This particularly high first reduction potential may explain the “spontaneous” reduction of the system that generates the above-mentioned ESR signal in solution and in the solid state.

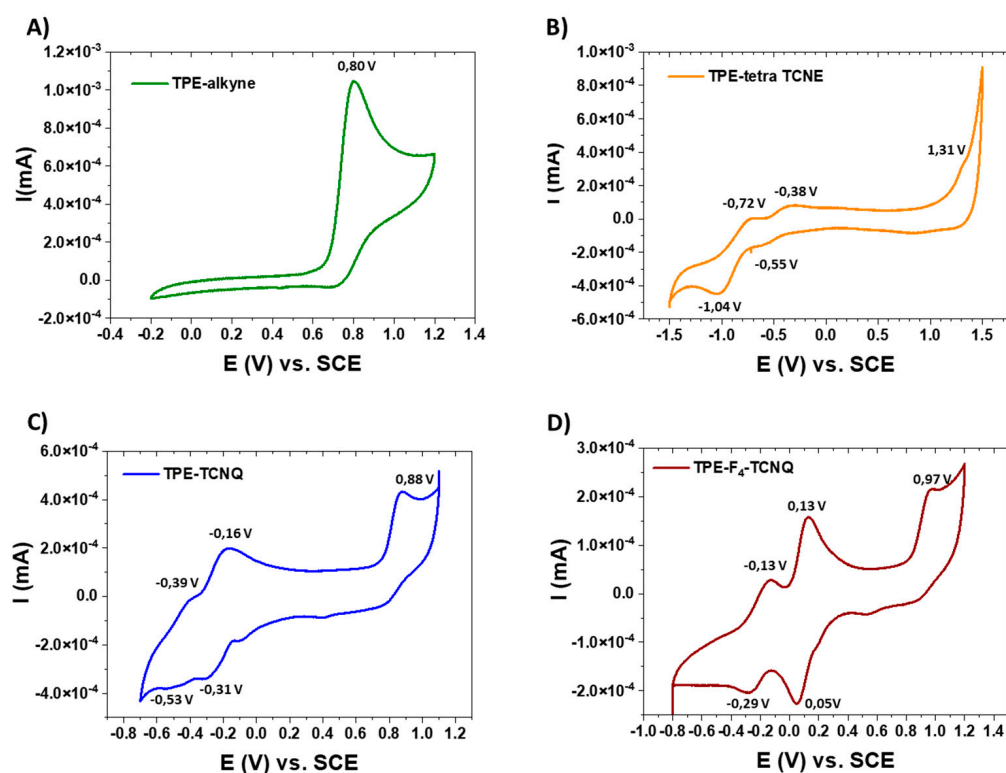


**Figure 7.** Cyclic voltammograms of TPE-alkyne (A), TPE-TCNE (B), TPE-TCNQ (C) and TPE-F<sub>4</sub>-TCNQ (D) in CH<sub>2</sub>Cl<sub>2</sub> + Bu<sub>4</sub>NPF<sub>6</sub> solutions. Scan rate: 100 mV.s<sup>-1</sup>, Pt disk working electrode. Potentials are given vs. SCE.

**Table 2.** Electrochemical data extracted from cyclic voltammetry in dichloromethane with 0.2 M of NBu<sub>4</sub>PF<sub>6</sub> as electrolyte (potentials versus saturate calomel electrode).

	TPE-Alkyne	TPE-TCNE	TPE-TCNQ	TPE-F <sub>4</sub> -TCNQ
$E_{1/2}$ (V) <sup>a</sup>	-	$-0.45$ $-0.88$	$-0.23$ $-0.46$	$+0.09$ $-0.21$
$E_p$ <sup>b</sup>	$+0.80$	$+1.31$	$+0.88$	$+0.97$

<sup>a</sup>  $E_{1/2} = (E_{pc} + E_{pa})/2$ , in which  $E_{pc}$  and  $E_{pa}$  correspond to the cathodic and anodic peak, respectively (this potential is calculated when the electron transfer is reversible) <sup>b</sup>  $E_p$  = potential peak (irreversible wave).



#### 2.4. Electronic Structure Calculations

To gain more insights into the photophysical and electrochemical measurements on the four TPE derivatives, theoretical calculations based on (Time-Dependent) Density Functional Theory (TD)-DFT were performed [90–94]. All calculations were carried out using the long-range hybrid CAM-B3LYP functional [95] and a 6-311G (d,p) basis set, as motivated by the fact that the DFT functionals with long-range corrections better describe excited states with a pronounced charge transfer character [96].

The shape of the frontier orbitals in the optimized structures obtained from the DFT calculations are displayed in Figure 8 (see also Figure S44). For TPE-alkyne, the HOMO is delocalized evenly on the entire molecule while the LUMO is denser on the TPE core. In TPE-TCNE, the HOMO is localized on the extremity of one TCBD arm following the introduction of an electron-accepting group in its center, thus breaking apart the large delocalization observed for the pristine compound. Similarly, the HOMO-1 to HOMO-3 levels get localized over the other branches (Figure S46). The LUMO spreads along a diagonal involving both the TPE core and the inner part of two TCBD arms. A similar pattern prevails for the LUMO + 1, while the LUMO + 2 and LUMO + 3 are delocalized over the other diagonal (Figure S46). In the case of TPE-TCNQ and TPE-F<sub>4</sub>-TCNQ, the frontier orbital spatial distribution is quite similar, with the HOMO and LUMO levels localized over the terminal donor part and inner acceptor part, respectively, of a single arm. The deeper occupied and higher unoccupied levels are localized over the other branches. Here, the TPE core is thus weakly involved in the frontier orbital distribution. Excited states with a pronounced intra- and/or interbranch character are thus expected at low energy. Since the molecular orbitals are not uniformly distributed over all branches, these frontier molecular orbitals are quasi-degenerate, particularly the HOMOs (see Figures S45 and S46).

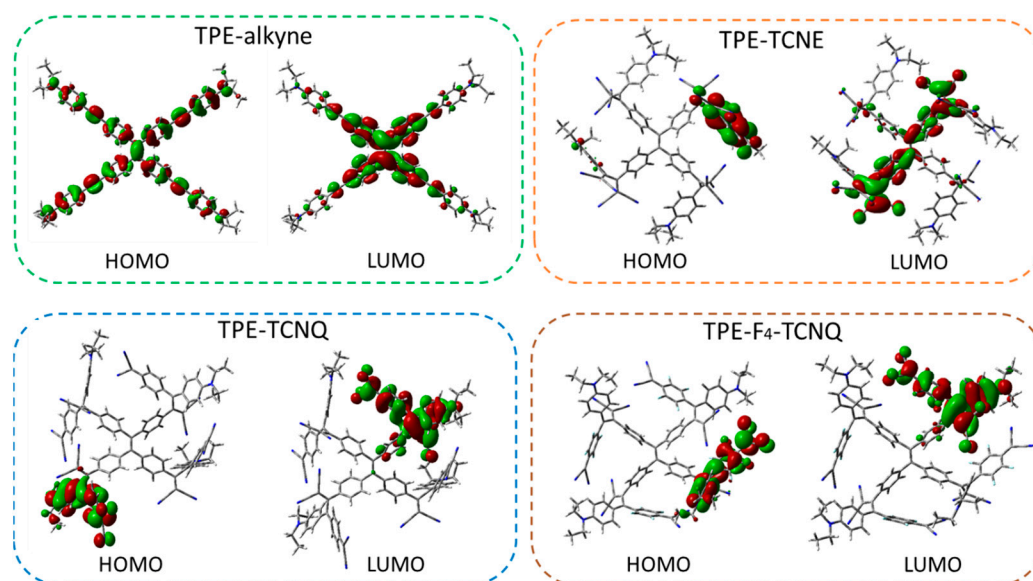


**Figure 8.** Frontier orbitals of the investigated compounds from the CAM-B3LYP/6.311g(d,p)-calculated optimized structures. Isovalues are set to  $0.02 e/\text{au}^3$ .

The relative energy level alignment of the frontier orbitals of the TPE adducts was estimated from the DFT calculations and are displayed in Figure 9 when accounting for the solvent effects (i.e., THF used for the optical absorption spectra) via the Polarizable Continuum Model (PCM). As measured in cyclic voltammetry, the calculated HOMO–LUMO gaps decrease when increasing the electron-withdrawing character of the adducts in the following order: F<sub>4</sub>-TCNQ > TCNQ > TCNE. It is worth remembering that the absolute values of the gap cannot be directly compared to the CV data since the calculations rely on Koopmans' approximation (associating the ionization potential to the HOMO of the neutral molecule and the electron affinity to the LUMO energy). Moreover, the

amplitude of the HOMO–LUMO gap critically depends on the choice of the DFT functional. Nevertheless, comparing the evolution of the HOMO and LUMO energies on a relative basis is meaningful. Doing so, we observe that the shift between the frontier energy levels of the various TPE adducts nicely matches the experimental trends (see Figure 9).

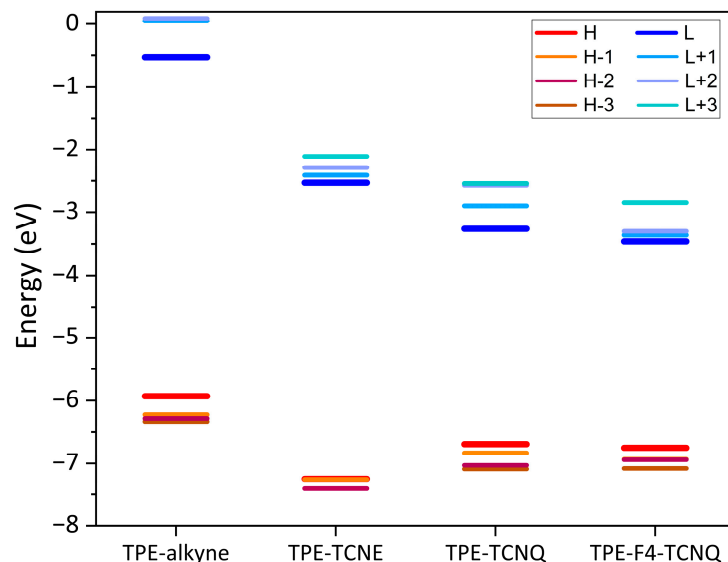


**Figure 9.** Energy level alignment of the four frontier occupied and virtual molecular orbitals for the investigated systems in THF, as calculated at the CAM-B3LYP/6-311G (d,p) level.

### 2.5. Excited-State Calculations

The absorption spectra of the TPE compounds simulated at the TD-DFT level using the same functional and base set are shown in Figure 10 (see also Figure S47). The Gaussian broadening used to generate the UV–Visible absorption spectra is set to  $\sigma = 0.25$  eV to match the width of the experimental bands. The computed electronic transitions, as well as their corresponding oscillator strength and assignment, are listed in Table S1, Supplementary Materials.

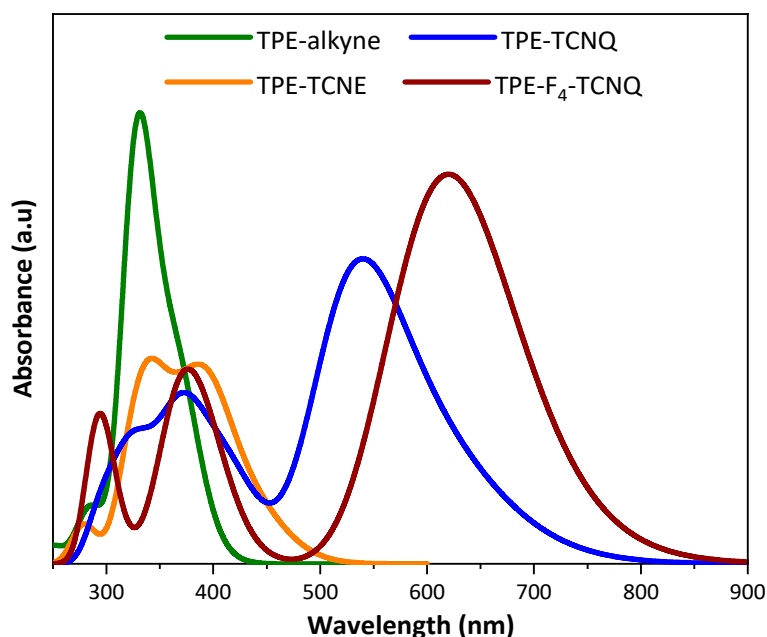


**Figure 10.** UV–Visible absorption spectra of the investigated compounds in THF simulated at the TD-DFT/CAM-B3LYP level.

For TPE-alkyne, the lowest excitation occurs at 367 nm, which is in very good agreement with the strong absorption band experimentally observed in its UV–Visible absorption spectrum ( $\lambda_{\max} = 359$  nm, Table 1, Figure 3). This corresponds to a transition from the HOMO to the LUMO level (see Table S1, Supplementary Materials). Conversely, the absorption spectra of the TPE adducts exhibit an additional absorption band with a CT character in the visible–near infrared region. For TPE-TCNE, TPE-TCNQ and TPE-F<sub>4</sub>-TCNQ, the lowest excitation occurs at 443 nm, 625 nm and 675 nm, respectively. To further analyze the nature of these excitations, we performed an NTO analysis that describes globally for each given excitation where the electron is excited from and where it is promoted during the excitation, i.e., as a single-particle transition from an effective occupied to virtual orbital [97]. We refer to the occupied and virtual NTOs as “hole” and “electron” transition orbitals, respectively. Note that the NTOs are not the same as the occupied and virtual molecular orbitals calculated in the ground state. Moreover, we have also calculated the spatial overlap  $\phi_s$  between the electron and hole density in order to quantitatively evaluate the charge-transfer character of an electronic transition;  $\phi_s = 1$  for a purely localized character and  $\phi_s = 0$  for a pure charge transfer excitation [98,99]. In the case of TPE-TCNE, the lowest excitation at 443 nm is predominantly assigned to a transition from a hole orbital localized on the extremity of a TCBD arm to an electron orbital localized on the inner part of the same TCBD arm and including a part of the TPE core. This graphical picture of NTOs is consistent with the moderate spatial overlap  $\phi_s$  value of 0.47 calculated for this transition (see Figure 11). Moving to TPE-TCNQ and TPE-F<sub>4</sub>-TCNQ, the dominant transition contributing to the lowest excitation at 625 nm and 675 nm, exhibits both a weaker charge-transfer character compared to TPE-TCNE due to the strong spatial overlap between the hole and electron NTO orbitals as evidenced by a larger  $\phi_s$  index (0.70 and 0.72, respectively) (see Figure 11). For all TPE adducts, the high oscillator strength associated with the lowest excitation is attributed to this strong intra-branch character. Interestingly, the simulated absorption spectra nicely reproduce the experimental bathochromic shift of the CT absorption band. Going from TPE-TCNE, TPE-TCNQ to TPE-F<sub>4</sub>-TCNQ, a systematic red shift in the CT absorption band as well as an increase in its intensity are noticed, which is fully in line with the increase in the electron-withdrawing strength of the TPE adducts and the decrease in the CT character, respectively. This red shift can be evaluated by computing the energy difference between the main peaks of the lowest charge transfer band of the TPE conducts. Thus, moving from TPE-TCNE ( $E_{\max} = 3.11$  eV) to TPE-TCNQ ( $E_{\max} = 2.27$  eV), a red shift of 0.84 eV is computed whereas a red shift of 0.34 eV is obtained going from TPE-TCNQ ( $E_{\max} = 2.27$  eV) to TPE-F<sub>4</sub>-TCNQ ( $E_{\max} = 1.93$  eV) (see Figure S46). These results are in excellent agreement with experiments showing the same red shifts of 0.84 eV and 0.34 eV, respectively (see Table 1).

### 2.6. Photothermal Properties and Thermal Stability

Due to their high absorption in the red-NIR region, TPE-TCNQ and TPE-F<sub>4</sub>-TCNQ appear as suitable photothermal agents, relaxing to their ground state non-radiatively by the creation of phonons (vibrations) and thus affording an increase in the temperature [100]. To investigate the photothermal behavior of TPE-TCNQ and TPE-F<sub>4</sub>-TCNQ, the temperature changes of thin films and powders under a laser beam were measured. Figure S23 shows absorption spectra for TPE-TCNE, TPE-TCNQ and TPE-F<sub>4</sub>-TCNQ thin films. A wavelength of 808 nm was selected for this study for two reasons: (i) this wavelength is in the first biological transparency window (NIR-I, 750–1000 nm), (ii) this wavelength is located in a good absorbing region of the UV–Visible absorption spectra of both molecules. In similar conditions, TPE-F<sub>4</sub>-TCNQ shows a stronger photothermal conversion compared to TPE-TCNQ (Figure 12). Figure 13 displays photothermal conversion cycles for TPE-F<sub>4</sub>-TCNQ at different laser powers. The thermal cycles are reproducible, indicating that the molecules do not degrade under irradiation (see Figure S40). The first cycle was fitted using the COMSOL software to extract the surface heat power produced by the beam light irradiation. In the case of thin films and at the maximum power of the laser (2.58 W/cm<sup>2</sup>),

the temperature rose to a maximum of 50 °C in less than one minute. If the thin film is replaced by a dense powder of TPE-F<sub>4</sub>-TCNQ, the temperature rises at almost 100 °C in less than one minute (Figure 13). This difference is explained by an increase in the amount of matter of the sample leading to an increase in light absorption in the case of the irradiation of the powder. Finally, to check the thermal stability of TPE-TCNQ and TPE-F<sub>4</sub>-TCNQ, a thermogravimetric analysis (TGA) under nitrogen flow was performed indicating no weight loss greater than 2% up to 320 °C (see Figure S36).

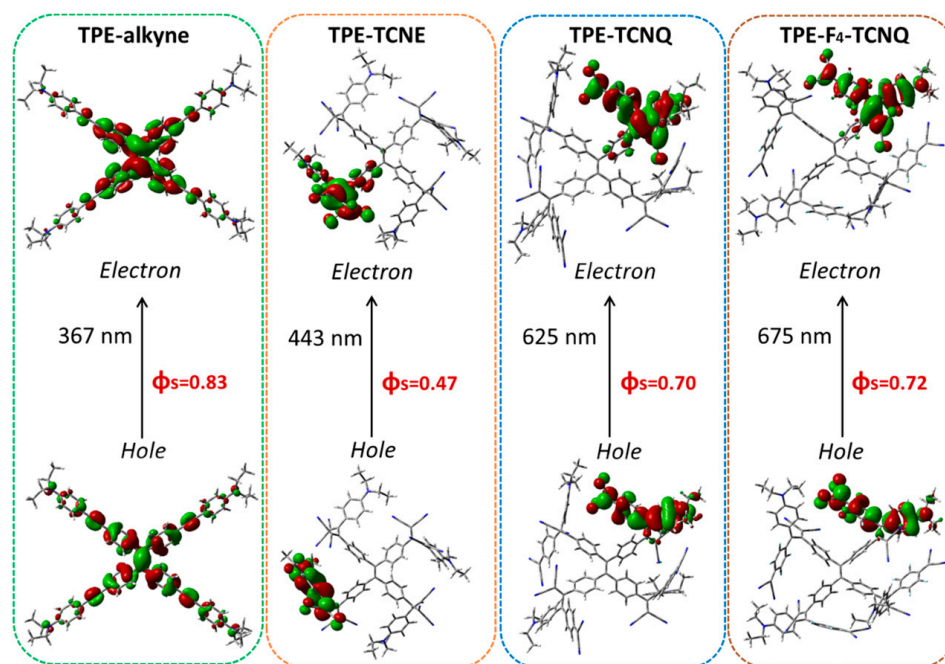


**Figure 11.** The hole and electron Natural Transition Orbitals (NTOs) for the lowest excitation of the investigated compounds with the associated energy, and  $\phi_s$  descriptor, computed at the CAM-B3LYP/6-311G(d,p). Isovalues are set to 0.02 e/au<sup>3</sup>.

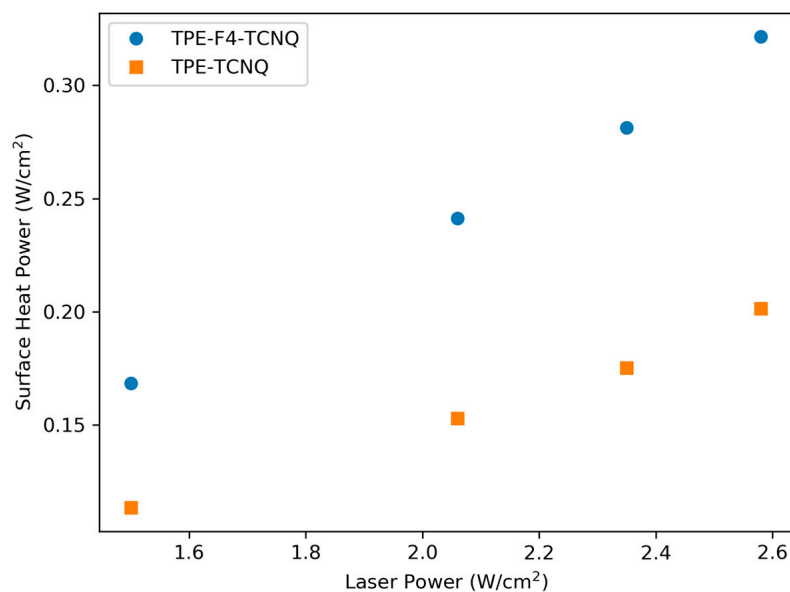


**Figure 12.** Comparison of the surface heat power vs. laser power at 808 nm for TPE-TCNQ (orange) and TPE-F<sub>4</sub>-TCNQ (blue) as thin films.

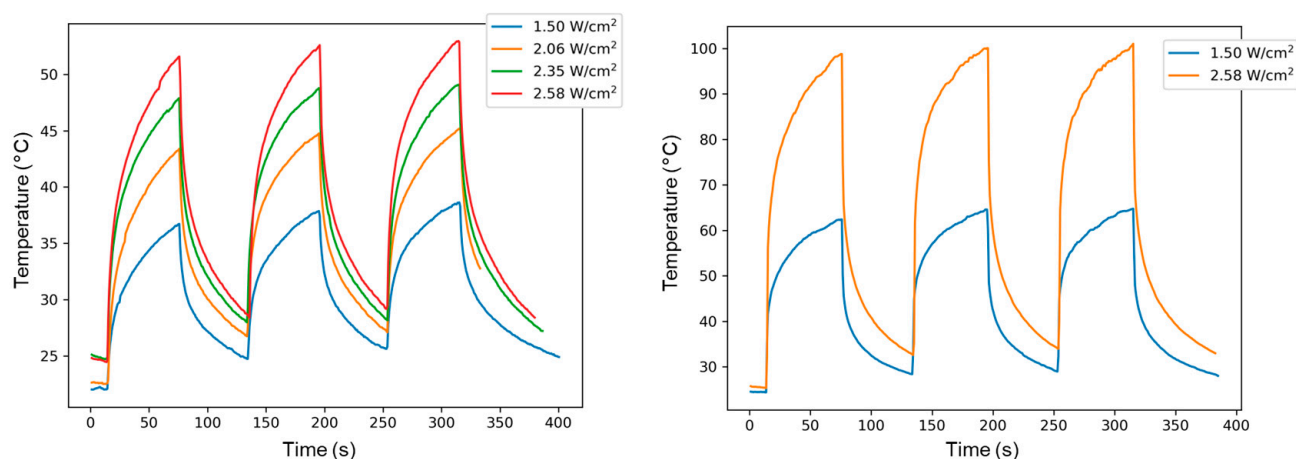


**Figure 13.** Photothermal conversion behavior of TPE-F<sub>4</sub>-TCNQ under 808 nm laser irradiation at different laser powers (1.50, 2.06, 2.35, and 2.58 cm<sup>-2</sup>), as a thin film (left) and as a powder (right).

### 2.7. Concluding Remarks

Generally speaking, it is interesting to note that almost all the CA-RE derivatives described in the literature to date have spectral characteristics extremely close to those described in this paper when the electron donating group is a dialkyl or a diphenyl aniline [54,57,59,62,69–74,76,83–86,101–117]. In all cases, the ICT bands are found in the same regions within a few nm. The CT band A is between 450 and 470 nm and the CT band B between 680 and 710 nm for TCNQ and between 830 and 860 nm for F<sub>4</sub>-TCNQ. This indicates that whatever the starting alkyne, the charge transfers will only involve the cyanated parts and the aniline. This supposition is well supported by the TD-DFT calculations that showed that the central core played a very negligible role in the frontier orbitals and thus in the electronic properties. The observed behavior is exclusively governed by the clicked moieties.

## 3. Methods and Materials

### 3.1. Materials

Dry tetrahydrofuran (THF), dichloromethane (DCM) and diethyl ether (Et<sub>2</sub>O) were obtained by using a solvent purification system Puresolve MD5 from Inert. Anhydrous N,N-dimethylformamide (DMF) (Acros, 99.8%), dichlorobenzene (TCI, 99%), anhydrous acetonitrile (Alfa Aesar, 99.8%) and absolute ethanol (VWR) were used as received. Triphenylphosphine (Fluorochem, 99%), *n*-tetrabutylammonium fluoride (Sigma-Aldrich, 1M in THF), 1,1,2,2-tetraphenylethene (TPE) (Fluorochem, 95%), bromine (Sigma-Aldrich, 99%), copper iodide (Alfa Aesar, 99.998%), 4-ethynyl-N,N-dimethylaniline (Aldrich, 97%), diisopropylamine (Aldrich, 99.5%), 4-iodoaniline (Alfa Aesar, 98%), 1-bromododecane (ABCR, 99%), trimethylsilylacetylene (Fluorochem, 99%), 4,4'-dibromobenzophenone (Fluorochem, 98%), titanium (IV) chloride (Merck, 97%), zinc dust (Aldrich, 98%), pyridine (Aldrich, 99.8%), tetracyanoethylene (TCNE) (Aldrich, 96%), 7,7,8,8-Tetracyanoquinodimethane (TCNQ) (Alfa Aesar, 98%), 2,3,5,6-Tetrafluoro-7,7,8,8-tetracyanoquinodimethane (F<sub>4</sub>-TCNQ) (Fluorochem, 95%) were used as received. Tetrakis(triphenylphosphine)-palladium (0) [Pd(PPh<sub>3</sub>)<sub>4</sub>], was prepared according to literature procedures [113]. Ph-I-N-C<sub>12</sub>, Ph-SiMe<sub>3</sub>-N-C<sub>12</sub> and Ph-alkyne were synthesized according to procedures described in the literature [114]. Reactions were monitored by thin-layer chromatography (TLC) using Merck® TLC Silica gel 60 F254 plates. Flash chromatography was carried out using a Biotage® Isolera™ System (UV-Vis 200 nm–800 nm detector) over silica cartridges (SNAP Ultra or Sfar HC D).

### 3.2. Characterization Methods

Unless otherwise stated, measurements were done on the equipment available at the Plateforme d'Analyse et Caractérisation (PAC) of the Balard Institute, CNRS, University of Montpellier, France.

IR spectra were carried out on a Perkin Elmer Spectrum 2 FT-IR instrument using the attenuated total reflectance (ATR) measurement mode (diamond crystal). The wavenumber range analyzed was 500–4000  $\text{cm}^{-1}$  and the optical resolution of the instrument was 4  $\text{cm}^{-1}$ .

$^1\text{H}$  NMR spectra were recorded at 273 K or 298 K on a Bruker Avance III 400 MHz NMR spectrometer using a BBFO probe or a Bruker Avance III 500 MHz NMR spectrometer using a Prodigy BBO Z-gradient CryoProbe or a Bruker Avance III 600 MHz NMR spectrometer using a Prodigy TCI Z-gradient CryoProbe and calibrated to TMS on the basis of the relative chemical shift of the residual non-deuterated solvent as an internal standard ( $\text{CD}_2\text{Cl}_2$ :  $\delta = 5.32$  ppm,  $\text{CDCl}_3$ :  $\delta = 7.26$  ppm,  $\text{DMSO-d}_6$ :  $\delta = 2.50$  ppm,  $\text{THF-d}_8$ :  $\delta = 3.58$  ppm).  $^{13}\text{C}\{^1\text{H}\}$  NMR spectra were recorded at 298 K on a Bruker Avance III 500 MHz NMR spectrometer using a Prodigy BBO Z-gradient CryoProbe or a Bruker Avance III 600 MHz NMR spectrometer using a Prodigy TCI Z-gradient CryoProbe and calibrated to TMS on the basis of the relative chemical shift of the residual non-deuterated solvent as an internal standard ( $\text{CD}_2\text{Cl}_2$ :  $\delta = 53.84$  ppm,  $\text{CDCl}_3$ :  $\delta = 77.16$  ppm,  $\text{DMSO-d}_6$ :  $\delta = 39.52$  ppm,  $\text{THF-d}_8$ :  $\delta = 67.21$  ppm).  $^{19}\text{F}$  NMR spectra were recorded at 298 K on a Bruker Avance III 400 MHz NMR spectrometer using a BBFO probe.

The MS (MALDI) spectra were recorded on a Rapiflex (Bruker) with Matrix-Assisted Laser Desorption Ionization (MALDI) source and a TOF analyzer. The mass spectra were recorded in positive mode between 500 and 15,000 Da in reflector mode for TPE-adduct. Samples were incorporated in a DCTB matrix. Mass accuracy measurement were done at UMONS, Organic Synthesis and Mass Spectrometry Laboratory (S2MOs, Mons, Belgium), by using a Waters QToF Premier mass spectrometer equipped with Matrix-Assisted Laser Desorption/Ionization source. A Nd-YAG laser of 355 nm with a maximum pulse energy of 65  $\mu\text{J}$  delivered to the sample at 50 Hz repeating rate is used. Time-of-flight mass analyses were performed in the reflection mode at a resolution of about 10 k ( $m/z$  569). Trans-2-(3-(4-tert-butyl-phenyl)-2-methyl-2-propenylidene)malononitrile (DCTB) was used as the matrix and was prepared as a 40 mg/mL solution in chloroform. The matrix solution (1  $\mu\text{L}$ ) was applied to a stainless-steel target and air-dried. Samples were dissolved in chloroform to obtain 1 mg/mL solutions. 1  $\mu\text{L}$  aliquots of these solutions were applied onto the target area (already bearing the matrix crystals) and air-dried. Exact mass was determined by using poly(ethylene glycol) as internal reference.

The UV-Visible absorption spectra were recorded on a JASCO V-650 spectrophotometer in 10 mm quartz cells (Hellma). The molar extinction coefficients ( $\epsilon$ ) were determined by the plot of absorbance vs. concentration by preparing solutions at different concentrations in THF. The concentration range was chosen to remain in the linear range of the Beer–Lambert relationship ( $A$  ca. 0.2–0.8).

The optical gap ( $E_g$ ) was determined by the Tauc method [115]. The onset wavelength of the absorption spectra was determined by the intersection of the straight line fitted to the right-hand side of the maximum with the baseline of the absorption.

Thin film were realized by deposition of ca.  $10^{-5}$  mol.l $^{-1}$  THF solutions on a quartz plate followed by the evaporation of the solvent. The operation was repeated until an absorbance of ca. 0.25 was measured at the maximum of the Intramolecular Charge Transfer (ICT) band.

The emission spectra in powder and in solution for TPE-TCNE, TPE-TCNQ and TPE-F $_4$ -TCNQ adducts were recorded in the Laboratoire de Chimie de l'ENS Lyon recorded on a fluorescence spectrofluorimeter (Fluorolog-3, Horiba-Jobin Yvon) equipped with R2658 photomultiplier tube (Hamamatsu, water cooling) or Synapse InGaAs/Symphony II (Horiba, nitrogen cooling) as detectors. The steady-state luminescence was excited by non-polarized light from a 450 W xenon CW lamp.

The measurement of quantum yields were carried out with an FLS980 integrating sphere (Edinburgh Instruments) connected to a FS920 fluorescence spectrophotometer (Edinburgh Instruments), equipped with a calibrated photomultiplier in a Peltier (air cooled) housing (R928P, Hamamatsu) operating up to 900 nm, with a 450 W continuous xenon arc lamp as the excitation source.

Measurements were performed in the Institut des Sciences Chimiques de Rennes – France (ISCR). For TPE-adducts, CVs were carried out on a  $10^{-3}$  mol.L $^{-1}$  solution of sample in CH<sub>2</sub>Cl<sub>2</sub>/[NBu<sub>4</sub>][PF<sub>6</sub>] 0.1 mol.L $^{-1}$ . CVs were recorded on a Biologic SP-50 instrument at 0.1 V s $^{-1}$  on a platinum disk electrode. Potentials were measured versus a KCl saturated calomel electrode (SCE).

ESR spectra were recorded on a Bruker Elexsys E500 CW continuous wave, X band (9.8 GHz) spectrometer equipped with ER4122 SHQ cavity at room temperature. Sample was diluted in THF and introduced in a quartz tube. The window was 10 mT (100 G) centered around  $g = 2$  with 2 G of amplitude modulation, 100 kHz of frequency modulation, 10 dB of micro-wave power and 70 dB of gain.

Thermogravimetric analyses (TGA) were carried out on a STA 449 F1 Jupiter Netzsch analyzer under dry nitrogen at a heating rate of 10 °C.min $^{-1}$ .

Photothermal measurements were realized on samples of TPE-TCNE and TPE-F<sub>4</sub>-TCNQ. Two different deposits were realized with both samples. First bulk materials (powders) were placed on a quartz surface. Secondly, thin films of both samples were deposited on quartz slide from diluted THF solutions (*ca.*  $1.10^{-4}$  mol.L $^{-1}$ ). Then, we used a 808 nm laser (Kamax society, Limoges, France) with an adjustable power from 0 to 2.58 W/cm<sup>2</sup>. The laser spot surface was 0.32 cm<sup>2</sup>. The temperature of the surface was measured using an OPTRIS PI 450 thermal camera (Media Mesures, Bouc Bel Air, France). The samples were deposited on a polystyrene surface in contact with air to limit heat transfer with the support.

Photothermal simulations were realized using the COMSOL software [116]. The heat equation was solved simultaneously with the simplified Navier–Stokes equation to take into account the heat propagation and the convection terms present for the air. The model consisted of a quartz substrate, with a surface heat source to simulate the heat produced by the laser absorption of the TPE-TCNQ or TPE-F<sub>4</sub>-TCNQ sample layer, deposited on a polystyrene support.

### 3.3. Calculations Details

The ground-state geometry of the molecules has been first optimized without any symmetry constraint in the gas phase and the electronic properties of the optimized structures have been next determined in gas phase, in THF and in DCM used in the CV measurements. The vibrational frequencies associated to the optimized structures were also calculated to verify that they correspond to local minima on the energy surface. The absorption spectra and the vertical electronic transitions have been next computed at the TD-DFT level and compared to the corresponding experimental data. All calculations have been carried out using the long-range hybrid Cam-B3LYP functional [117] and a 6-311G (d,p) basis set within Revision D.01 of the Gaussian 09 program package [5]. The solvent effects in THF, used for the spectroscopic measurements, were simulated by means of the polarizable continuum model (PCM) [118].

### 3.4. Synthesis

**Bz-alkyne.** 4,4'-dibromobenzophenone (0.90 g, 2.66 mmol) was introduced into a 100 mL two neck round-bottom flask under argon atmosphere with 30 mL of anhydrous THF. Copper (I) iodide (20 mg, 0.11 mmol, 4 mol%), bis(triphenylphosphine)palladium (II) chloride (77 mg, 0.11 mmol, 4 mol%) and triphenylphosphine (13 mg, 0.05 mmol, 2 mol%) were then added (solution 1). In parallel, Ph-alkyne (2.90 g, 6.38 mmol, 2.4 eq) was introduced into a Schlenk tube under argon atmosphere with 10 mL of anhydrous THF and 20 mL of diisopropylamine (solution 2). Once prepared, solution 2 was transferred

into solution 1 through cannula. The mixture was then heated to 65 °C overnight. Once judged complete, the solvent was removed under reduced pressure. The crude mixture was first filtrated on a silica gel column chromatography with cyclohexane before being purified by column chromatography on silica gel using gradient elution (100% cyclohexane to 70% cyclohexane / 30% dichloromethane). The fraction corresponding to the product was concentrated and then, diluted with a mixture of dichloromethane (5 mL) and acetone (50 mL). The solution was cooled. The resulting precipitate was filtered leading to Bz-alkyne as a yellow-orange powder. Yield 73% (2.10 g, 1.93 mmol). FTIR-ATR ( $\text{cm}^{-1}$ ): 2202 ( $\nu\text{C}\equiv\text{C}$ ), 1651 ( $\nu\text{C}=\text{O}$ ).  $^1\text{H}$  NMR (500 MHz,  $\text{CD}_2\text{Cl}_2$ ,  $\delta$ ): 7.75 (d, 4H,  $^3J_{\text{H-H}} = 8.5$  Hz), 7.58 (d, 4H,  $^3J_{\text{H-H}} = 8.5$  Hz), 7.37 (d, 4H,  $^3J_{\text{H-H}} = 9.0$  Hz), 6.60 (d, 4H,  $^3J_{\text{H-H}} = 9.0$  Hz), 3.29 (t, 8H,  $^3J_{\text{H-H}} = 7.7$  Hz), 1.63–1.55 (m, 8H), 1.37–1.21 (m, 72H), 0.88 (t, 12H,  $^3J_{\text{H-H}} = 7.0$  Hz) ppm.  $^{13}\text{C}\{^1\text{H}\}$  NMR (126 MHz,  $\text{CD}_2\text{Cl}_2$ ,  $\delta$ ): 195.3, 148.9, 136.3, 133.5, 131.2, 130.5, 129.2, 111.6, 108.0, 95.2, 87.2, 51.4, 32.5, 30.2, 30.2, 30.1, 30.0, 29.9, 27.6, 27.6, 23.2, 14.4 ppm. HRMS (Maldi, DCTB):  $m/z$   $[\text{M}]^{+\bullet}$  calc for  $[\text{C}_{77}\text{H}_{116}\text{N}_2\text{O}]^{+\bullet}$ : 1084.9088; found: 1084.9081 ( $\delta = 0.6$  ppm).

**TPE-alkyne.** Bz-alkyne (600 mg, 0.55 mmol) and zinc dust (111 mg, 1.70 mmol, 3 eq) were dissolved in anhydrous THF (30 mL) into a 100 mL three neck round bottom flask under argon atmosphere. Titanium (IV) chloride (120  $\mu\text{L}$ , 1.11 mmol, 2 eq) was added dropwise at  $-78$  °C. After return at room temperature, pyridine (20  $\mu\text{L}$ , 0.44 mmol, 0.4 eq/ $\text{TiCl}_4$ ) was added and the solution was stirred during 30 min at room temperature. The mixture was then heated at 65 °C overnight. The progress of the reaction was followed by TLC using *n*-hexane 96%/4% dichloromethane as eluent. When judged complete, the mixture was cooled at room temperature and then, quenched with of a 10% aqueous solution of  $\text{K}_2\text{CO}_3$  (60 mL). The aqueous layer was extracted with dichloromethane ( $5 \times 50$  mL). The organic layer was then dried over anhydrous  $\text{MgSO}_4$  and the solvent was removed under reduced pressure. The crude product was purified by column chromatography on silica gel using isocratic elution (90% *n*-hexane/9% dichloromethane/1% triethylamine). The product was isolated as an orange oil. Yield: 312 mg (0.15 mmol, 53%). FTIR-ATR ( $\text{cm}^{-1}$ ): 2208 ( $\nu\text{C}\equiv\text{C}$ ).  $^1\text{H}$  NMR (500 MHz,  $\text{CDCl}_3$ ,  $\delta$ ): 7.33 (d, 8H,  $^3J_{\text{H-H}} = 8.4$  Hz), 7.25 (d, 8H,  $^3J_{\text{H-H}} = 8.4$  Hz), 6.98 (d, 8H,  $^3J_{\text{H-H}} = 7.8$  Hz), 6.55 (d, 8H,  $^3J_{\text{H-H}} = 7.8$  Hz), 3.25 (t, 16H,  $^3J_{\text{H-H}} = 7.4$  Hz), 1.62–1.54 (m, 16H), 1.36–1.22 (m, 160H), 1.36–1.22 (t, 24H,  $^3J_{\text{H-H}} = 7.0$  Hz) ppm.  $^{13}\text{C}\{^1\text{H}\}$  NMR (126 MHz,  $\text{CDCl}_3$ ,  $\delta$ ): 148.0, 142.6, 140.8, 133.0, 131.6, 130.9, 122.7, 111.3, 108.9, 91.6, 87.3, 51.1, 32.1, 29.8, 29.8, 29.7, 29.5, 27.4, 27.3, 22.9, 14.3 ppm. HRMS (Maldi, DCTB)  $m/z$ :  $[\text{M}]^{+\bullet}$  calc for  $[\text{C}_{154}\text{H}_{232}\text{N}_4]^{+\bullet}$ : 2137.8277; found: 2137.8262 ( $\delta = -0.7$  ppm). UV-Vis (THF):  $\lambda$  ( $\epsilon$ ,  $\text{L}\cdot\text{mol}^{-1}\cdot\text{cm}^{-1}$ ) = 359 (143 400), 294 (82 400) nm.

**TPE-TCNE.** TPE-alkyne (74 mg, 35.0  $\mu\text{mol}$ ) was introduced into a Schlenk tube under argon atmosphere. 10 mL of anhydrous dichloromethane as well as tetracyanoethylene (TCNE, 27 mg, 0.21 mmol, 6 eq) were added. The solution was stirred at room temperature during 1 h. The progress of the reaction was followed by TLC using *n*-hexane/ $\text{CH}_2\text{Cl}_2$  (90/10 *v/v*) as eluent. When judged complete, the solvent was removed under vacuum. The product was then purified by column chromatography on silica gel using a gradient elution (90% *n*-hexane/10% dichloromethane to 80% *n*-hexane/20% dichloromethane). TPE-TCNE was isolated as a dark red film-forming solid. Yield: 65 mg (24  $\mu\text{mol}$ , 70%). FTIR-ATR ( $\text{cm}^{-1}$ ): 2213 ( $\nu\text{C}\equiv\text{N}$ ).  $^1\text{H}$  NMR (500 MHz,  $\text{CDCl}_3$ ,  $\delta$ ): 7.76 (d, 8H,  $^3J_{\text{H-H}} = 9.0$  Hz), 7.54 (d, 8H,  $^3J_{\text{H-H}} = 8.5$  Hz), 7.14 (d, 8H,  $^3J_{\text{H-H}} = 8.5$  Hz), 6.70 (d, 8H,  $^3J_{\text{H-H}} = 9.0$  Hz), 3.40 (t, 16H,  $^3J_{\text{H-H}} = 7.6$  Hz), 1.64 (q, 16H,  $^3J_{\text{H-H}} = 6.2$  Hz), 1.38–1.22 (m, 144H), 0.88 (t, 24H,  $^3J_{\text{H-H}} = 6.8$  Hz).  $^{13}\text{C}\{^1\text{H}\}$  NMR (126 MHz,  $\text{CDCl}_3$ ,  $\delta$ ): 168.8, 162.0, 153.5, 146.6, 142.8, 133.1, 132.3, 132.0, 129.9, 117.6, 114.9, 114.1, 112.6, 112.2, 111.3, 87.7, 51.7, 32.1, 29.8, 29.7, 29.6, 29.5, 27.5, 27.2, 22.8, 14.3 ppm. HRMS (Maldi, DCTB)  $m/z$ :  $[\text{M}]^{+\bullet}$  calc for  $[\text{C}_{178}\text{H}_{232}\text{N}_{20}]^{+\bullet}$ : 2649.8769; found: 2649.8757 ( $\delta = -0.5$  ppm). UV-Vis (THF):  $\lambda$  ( $\epsilon$ ,  $\text{L}\cdot\text{mol}^{-1}\cdot\text{cm}^{-1}$ ) = 469 (113 400), 307 (45 600) nm. Mp: 124–127 °C.

**TPE-TCNQ.** TPE-alkyne (100 mg, 47.0  $\mu\text{mol}$ , 1 eq) was introduced into a Schlenk tube under argon atmosphere with dichlorobenzene (10 mL). 7,7,8,8-tetracyano-*p*-quinodimethane (TCNQ, 57.6 mg, 0.28 mmol, 6 eq) was added. The solution was stirred at 100 °C during 1 h. The progress of the reaction was followed by TLC using *n*-hexane/ $\text{CH}_2\text{Cl}_2$  (90/10 *v/v*)



as eluent. The solvent was removed under vacuum. The residue was purified by column chromatography on silica gel with a gradient elution (90% *n*-hexane/10% dichloromethane to 80% *n*-hexane/20% dichloromethane). TPE-TCNQ was isolated as a dark film-forming solid. Yield: 66 mg (22.0  $\mu\text{mol}$ , 47%). FTIR-ATR ( $\text{cm}^{-1}$ ): 2201 ( $\nu\text{C}\equiv\text{N}$ ).  $^1\text{H}$  NMR (600 MHz, 273K,  $\text{CD}_2\text{Cl}_2$ ,  $\delta$ ): 7.46 (d, 4H,  $^3J_{\text{H-H}} = 8.0$  Hz), 7.43 (d, 8H,  $^3J_{\text{H-H}} = 8.6$  Hz), 7.28 (d, 8H,  $^3J_{\text{H-H}} = 9.1$  Hz), 7.20 (d, 4H,  $^3J_{\text{H-H}} = 8.1$  Hz), 7.04 (d, 12H,  $^3J_{\text{H-H}} = 8.6$  Hz), 6.93–6.81 (m, 4H), 6.71 (d, 8H,  $^3J_{\text{H-H}} = 9.1$  Hz), 3.38 (t, 16H,  $^3J_{\text{H-H}} = 7.7$  Hz), 1.65–1.60 (m, 16H), 1.38–1.18 (m, 144H), 0.88 (t, 24H,  $^3J_{\text{H-H}} = 6.9$  Hz) ppm.  $^{13}\text{C}\{^1\text{H}\}$  NMR (151 MHz, 273K,  $\text{CD}_2\text{Cl}_2$ ,  $\delta$ ): 172.5, 154.1, 152.2, 152.1, 146.3, 142.7, 136.4, 135.7, 135.1, 132.3, 131.0, 129.8, 124.7, 124.0, 115.9, 115.8, 113.6, 112.9, 112.5, 88.8, 51.7, 32.3, 30.0, 30.0, 30.0, 29.8, 27.6, 27.2, 23.1, 14.4 ppm. HRMS (Maldi, DCTB)  $m/z$ :  $[\text{M}]^{\bullet+}$  calc for  $[\text{C}_{202}\text{H}_{248}\text{N}_{20}]^{\bullet+}$ : 2954.0021; found: 2953.9946 ( $\delta = -2.5$  ppm). UV-Vis (THF)  $\lambda$  ( $\epsilon$ ,  $\text{L}\cdot\text{mol}^{-1}\cdot\text{cm}^{-1}$ ) = 688 (155 000), 468 (78 500), 337 (113 900) nm. Mp: 115–119  $^\circ\text{C}$ .

**TPE-F<sub>4</sub>-TCNQ.** TPE-alkyne (100 mg, 47.0  $\mu\text{mol}$ ) was introduced into a Schlenk tube under argon atmosphere with dichlorobenzene (10 mL). 2,3,5,6-Tetrafluoro-7,7,8,8-tetracyanoquinodimethane (F<sub>4</sub>-TCNQ, 77.9 mg, 0.28 mmol, 6 eq) was added. The solution was stirred at 100  $^\circ\text{C}$  during 1 h. The progress of the reaction was followed by TLC using 20% *n*-hexane/80% dichloromethane as eluent. The solvent was removed under vacuum. The product was purified by column chromatography on silica gel with a gradient elution (20% *n*-hexane/80% dichloromethane to 100% dichloromethane). TPE-F<sub>4</sub>TCNQ was isolated as a dark film-forming solid. Yield: 55 mg (22.0  $\mu\text{mol}$ , 36%). FTIR-ATR ( $\text{cm}^{-1}$ ): 2196 ( $\nu\text{C}\equiv\text{N}$ ).  $^1\text{H}$  NMR (400 MHz,  $\text{CDCl}_3$ ,  $\delta$ ): 7.51–7.29 (m, 16H), 7.15–6.99 (m, 8H), 6.90 (d, 8H,  $^3J_{\text{H-H}} = 8.1$  Hz), 3.74–3.50 (m, 16H), 1.83–1.70 (m, 16H), 1.35–1.19 (m, 144H), 0.88 (t, 24H,  $^3J_{\text{H-H}} = 6.8$  Hz) ppm.  $^{13}\text{C}\{^1\text{H}\}$  NMR (126 MHz,  $\text{CDCl}_3$ ,  $\delta$ ): 172.0, 156.5, 146.6, 146.1, 145.6, 143.5, 142.8, 140.5, 138.8, 138.5, 134.4, 133.7, 132.0, 130.1, 117.5, 116.3, 113.3, 113.1, 112.1, 107.3, 89.4, 53.5, 53.4, 32.0, 29.8, 29.7, 29.7, 29.6, 29.4, 28.5, 27.1, 22.8, 14.3 ppm.  $^{19}\text{F}$  NMR (376 MHz,  $\text{CDCl}_3$ ,  $\delta$ ): -134.1, -134.4, -143.1, 143.4 ppm. HRMS (Maldi, DCTB)  $m/z$ :  $[\text{M}]^{\bullet+}$  calc for  $[\text{C}_{202}\text{H}_{232}\text{F}_{16}\text{N}_{20}]^{\bullet+}$ : 3241.8513; found: 3241.8586 ( $\delta = 2.3$  ppm). UV-Vis (THF)  $\lambda$  ( $\epsilon$ ,  $\text{L}\cdot\text{mol}^{-1}\cdot\text{cm}^{-1}$ ) = 849 (163 400), 497 (73 600), 348 (97 500) nm. Mp: 160–164  $^\circ\text{C}$ .

#### 4. Conclusions

In conclusion, we have successfully applied the [2 + 2] CA-RE click reactions to a TPE platform adequately functionalized with electron-rich alkynes to obtain three cycloadducts, namely TPE-TCNE, TPE-TCNQ and TPE-F<sub>4</sub>-TCNQ. All these cycloadducts were fully characterized by NMR spectroscopy and HR-MS spectrometry. As confirmed by ESR spectroscopy, TPE-F<sub>4</sub>-TCNQ showed a substantial paramagnetic behavior in the solid state. As reported elsewhere, all compounds exhibited strong absorption bands in the NIR region of their UV-Visible absorption spectra, whose positions depend on the electron-withdrawing character of the clicked moieties. The origin of these bands was attributed by TD-DFT calculations to intramolecular charge transfers within the clicked moieties, indicating that the TPE core played a negligible role in the frontier orbitals and thus in the electronic properties. As a result, the TPE-alkyne precursor was rather luminescent, with a QY of 21%, and displayed a marked AIE behavior, whereas, among the clicked compounds, only TPE-TCNE showed a very faint fluorescence accompanied by an AIE behavior. Because they are non-luminescent and their CT band is in the NIR domain, TPE-TCNQ and TPE-F<sub>4</sub>-TCNQ were found to be suitable candidates for photothermal studies. Upon irradiation with a laser beam at 808 nm, both compounds exhibited excellent photothermal properties; the best results being obtained with powders of TPE-F<sub>4</sub>-TCNQ. In this case, a temperature of 100  $^\circ\text{C}$  was reached within less than one minute without decomposition under a laser power of 2.58  $\text{W}/\text{cm}^2$ . The present study shows that CA-RE click reactions provide an excellent strategy for conferring high performance photothermal properties to any molecular platform with appropriate functionalities and adequate thermal stability. This result is very interesting since it suggests that every already published or future CA-RE derivatives of TCNQ or F<sub>4</sub>-TCNQ could be good candidates for photothermal applications.

**Supplementary Materials:** The following supporting information can be downloaded at: <https://www.mdpi.com/article/10.3390/ijms24108715/s1>.

**Author Contributions:** Conceptualization, supervision and writing, S.C. and P.G.; synthesis, M.R. and S.R.; electrochemistry and spectroelectrochemistry, Y.B., Y.T. and A.V.; TD-DFT calculations, I.A. and J.C.; photothermal measurements, G.F.; HR-MS characterizations, J.D.W. All authors have read and agreed to the published version of the manuscript.

**Funding:** This research was funded by the Ministère de l'Enseignement Supérieur, de la Recherche et de l'Innovation (MESRI) and by the Centre National de la Recherche Scientifique (CNRS).

**Data Availability Statement:** Data is available in the Supplementary Material.

**Acknowledgments:** P.G. and S.C. also thank Saad Séne for fruitful discussions and the staff of Plateau d'Analyse et de Caractérisation (PAC) of the Pole Balard of Montpellier for the spectral and thermal characterizations. The computational facilities in Mons are provided by the Consortium des Équipements de Calcul Intensif (CÉCI) funded by the Belgian National Fund for Scientific Research (F.R.S.-FNRS) for providing the computational resources. J.C. is an FNRS research director.

**Conflicts of Interest:** The authors declare no conflict of interest.

## References

1. Braye, E.H.; Hübel, W.; Caplier, I. New Unsaturated Heterocyclic Systems. I. *J. Am. Chem. Soc.* **1961**, *83*, 4406–4413. [[CrossRef](#)]
2. Luo, J.; Xie, Z.; Lam, J.W.; Cheng, L.; Chen, H.; Qiu, C.; Kwok, H.S.; Zhan, X.; Liu, Y.; Zhu, D.; et al. Aggregation-induced emission of 1-methyl-1,2,3,4,5-pentaphenylsilole. *Chem. Commun.* **2001**, *18*, 1740–1741. [[CrossRef](#)] [[PubMed](#)]
3. Xia, Q.; Zhang, Y.; Li, Y.; Li, Y.; Li, Y.; Feng, Z.; Fan, X.; Qian, J.; Lin, H. A historical review of aggregation-induced emission from 2001 to 2020: A bibliometric analysis. *Aggregate* **2022**, *3*, e152. [[CrossRef](#)]
4. Zhao, Z.; Zhang, H.; Lam, J.W.Y.; Tang, B.Z. Aggregation-Induced Emission: New Vistas at the Aggregate Level. *Angew. Chem. Int. Ed. Engl.* **2020**, *59*, 9888–9907. [[CrossRef](#)]
5. Zhang, H.; Liu, J.; Du, L.; Ma, C.; Leung, N.L.C.; Niu, Y.; Qin, A.; Sun, J.; Peng, Q.; Sung, H.H.Y.; et al. Drawing a clear mechanistic picture for the aggregation-induced emission process. *Mater. Chem. Front.* **2019**, *3*, 1143–1150. [[CrossRef](#)]
6. Zhang, H.; Zhao, Z.; Turley, A.T.; Wang, L.; McGonigal, P.R.; Tu, Y.; Li, Y.; Wang, Z.; Kwok, R.T.K.; Lam, J.W.Y.; et al. Aggregate Science: From Structures to Properties. *Adv. Mater.* **2020**, *32*, 2001457. [[CrossRef](#)] [[PubMed](#)]
7. Xu, S.; Duan, Y.; Liu, B. Precise Molecular Design for High-Performance Luminogens with Aggregation-Induced Emission. *Adv. Mater.* **2020**, *32*, 1903530. [[CrossRef](#)]
8. Wan, Q.; Li, Y.; Ding, K.; Xie, Y.; Fan, J.; Tong, J.; Zeng, Z.; Li, Y.; Zhao, C.; Wang, Z.; et al. Aggregation Effect on Multiperformance Improvement in Aryl-Armed Phenazine-Based Emitters. *J. Am. Chem. Soc.* **2023**, *145*, 1607–1616. [[CrossRef](#)]
9. Jiang, W.; Zhang, G.; Zhao, G.; Wang, X.; Tian, W.; Sun, Y. Novel benzonitrile-based AIE host with high triplet energy for highly efficient solution-processed blue TADF OLEDs. *Dyes Pigm.* **2023**, *210*, 111037. [[CrossRef](#)]
10. Hwang, J.; Nagaraju, P.; Cho, M.J.; Choi, D.H. Aggregation-induced emission luminogens for organic light-emitting diodes with a single-component emitting layer. *Aggregate* **2023**, *4*, e199. [[CrossRef](#)]
11. Amro, K.; Thakur, A.K.; Rolland, M.; Van Der Lee, A.; Lemaur, V.; Lazzaroni, R.; Rault-Berthelot, J.; Poriol, C.; Hirsch, L.; Clément, S.; et al. Linking triptycene to silole: A fruitful association. *Mater. Chem. Front.* **2020**, *4*, 2006–2017. [[CrossRef](#)]
12. Anitha, O.; Mathivanan, M.; Tharmalingam, B.; Thirupathiraja, T.; Ghorai, S.; Natarajan, R.; Thiagarajan, V.; Lakshmiipathi, S.; Murugesapandian, B. Multi-stimuli responsiveness of pyrimidine bis-hydrazone: AIE, tuneable luminescence, white light emission, mechanochromism, acidochromism and its anticounterfeiting applications. *Dyes Pigm.* **2023**, *212*, 111091. [[CrossRef](#)]
13. Guo, X.; Song, T.; Chen, D.; Zhu, J.; Li, Z.; Xia, Q.; Wang, L.; Yang, W. Multi Stimuli-Responsive Aggregation-Induced Emission Active Polymer Platform Based on Tetraphenylethylene-Appended Maleic Anhydride Terpolymers. *ACS Appl. Mater. Interfaces* **2023**, *15*, 3543–3557. [[CrossRef](#)]
14. Deng, D.-D.; Zou, Y.; Chen, Z.; Liu, S.; Yang, Y.; Pu, S. Finely regulated benzothiadiazole derivatives: Aggregation-induced emission (AIE), hypso- or bathochromic mechanofluorochromic behaviors, and multilevel information encryption applications. *Dyes Pigm.* **2023**, *211*, 111051. [[CrossRef](#)]
15. Ahangar, A.A.; Ahmad, I.; Dar, A.A. AIE in the halogenated anils and their utilization as fluorescent probes for explosive nitro-aromatics. *New J. Chem.* **2023**, *47*, 4775–4783. [[CrossRef](#)]
16. Amro, K.; Clément, S.; Déjardin, P.; Douglas, W.E.; Gerbier, P.; Janot, J.-M.; Thami, T. Supported thin flexible polymethylhydrosiloxane permeable films functionalised with silole groups: New approach for detection of nitroaromatics. *J. Mater. Chem.* **2010**, *20*, 7100–7103. [[CrossRef](#)]
17. Zhang, Q.; Yin, B.; Hao, J.; Ma, L.; Huang, Y.; Shao, X.; Li, C.; Chu, Z.; Yi, C.; Wong, S.H.D.; et al. An AIEgen/graphene oxide nanocomposite (AIEgen@GO)-based two-stage “turn-on” nucleic acid biosensor for rapid detection of SARS-CoV-2 viral sequence. *Aggregate* **2023**, *4*, e195. [[CrossRef](#)] [[PubMed](#)]

18. Xu, R.; Zhang, P.; Shen, Q.; Zhou, Y.; Wang, Z.; Xu, Y.; Meng, L.; Dang, D.; Ben, Z.T. AIE nanocrystals: Emerging nanolights with ultra-high brightness for biological application. *Coord. Chem. Rev.* **2023**, *477*, 214944. [[CrossRef](#)]
19. Luo, W.; Tan, Y.; Gui, Y.; Yan, D.; Wang, D.; Tang, B.Z. Near-Infrared-Emissive AIE Bioconjugates: Recent Advances and Perspectives. *Molecules* **2022**, *27*, 3914. [[CrossRef](#)]
20. Wang, Z.; Zhou, Y.; Xu, R.; Xu, Y.; Dang, D.; Shen, Q.; Meng, L.; Tang, B.Z. Seeing the unseen: AIE luminogens for super-resolution imaging. *Coord. Chem. Rev.* **2022**, *451*, 214279. [[CrossRef](#)]
21. Yan, D.; Qin, Y.; Yan, S.; Sun, P.; Wang, Y.; Wang, D.; Tang, B.Z. Near-infrared emissive AIE nanoparticles for biomedical applications: From the perspective of different nanocarriers. *Particuology* **2023**, *74*, 103–118. [[CrossRef](#)]
22. Chua, M.H.; Chin, K.L.O.; Loh, X.J.; Zhu, Q.; Xu, J. Aggregation-Induced Emission-Active Nanostructures: Beyond Biomedical Applications. *ACS Nano* **2023**, *17*, 1845–1878. [[CrossRef](#)] [[PubMed](#)]
23. Ingle, J.; Basu, S. Mitochondria Targeted AIE Probes for Cancer Phototherapy. *ACS Omega* **2023**, *8*, 8925–8935. [[CrossRef](#)] [[PubMed](#)]
24. Yang, J.; Wang, Z.; Ge, J.; Deng, Y.; Ding, F.; Hu, L.; Wang, H. A deep-red emission AIE fluorescent probes based on coumarin for imaging lipid droplets in living cells. *J. Mol. Struct.* **2023**, *1277*, 134847. [[CrossRef](#)]
25. Ingle, J.; Sengupta, P.; Basu, S. Illuminating Sub-Cellular Organelles by Small Molecule AIEgens. *ChemBioChem* **2023**, *24*, e202200370. [[CrossRef](#)]
26. Huang, X.; Zhang, S.; Liu, Z.; Cao, W.; Li, G.; Gao, W.; Tang, B. Novel AIE Probe for In Situ Imaging of Protein Sulfonation to Assess Cigarette Smoke-Induced Inflammatory Damage. *Anal. Chem.* **2023**, *95*, 1967–1974. [[CrossRef](#)]
27. Kotras, C.; Fosseppe, M.; Roger, M.; Gervais, V.; Richeter, S.; Gerbier, P.; Ulrich, S.; Surin, M.; Clement, S. A cationic tetraphenylethene as a light-up supramolecular probe for DNA G-quadruplexes. *Front. Chem.* **2019**, *7*, 493. [[CrossRef](#)]
28. Arribat, M.; Remond, E.; Richeter, S.; Gerbier, P.; Clement, S.; Cavelier, F. Silole amino acids with aggregation-induced emission features synthesized by hydrosilylation. *Eur. J. Org. Chem.* **2019**, *2019*, 2275–2281. [[CrossRef](#)]
29. Pan, Z.; Wang, Y.; Chen, N.; Cao, G.; Zeng, Y.; Dong, J.; Liu, M.; Ye, Z.; Li, Y.; Huang, S.; et al. Aggregation-Induced emission photosensitizer with lysosomal response for photodynamic therapy against cancer. *Bioorg. Chem.* **2023**, *132*, 106349. [[CrossRef](#)]
30. Wang, X.; Xue, K.; Wang, X.; Zhao, Y.; Deng, J.; Yang, L.; Liang, J.; Li, Y.; Qi, Z. An aggregation-induced emission photosensitizer with efficient singlet oxygen generation capacity for mitochondria targeted photodynamic therapy. *Dyes Pigm.* **2023**, *213*, 111181. [[CrossRef](#)]
31. Zhou, L.; Chen, L.; Chen, S.; Pu, Z.; Gu, M.; Shen, Y. Highly Efficient Photodynamic Therapy with Mitochondria-Targeting Aggregation-Induced Emission Photosensitizer for Retinoblastoma. *Adv. Healthc. Mater.* **2023**, *12*, 2202219. [[CrossRef](#)]
32. Qu, R.; Zhen, X.; Jiang, X. Emerging designs of aggregation-induced emission agents for enhanced phototherapy applications. *CCS Chem.* **2022**, *4*, 401–419. [[CrossRef](#)]
33. Lin, Y.; Yi, M.; Guan, X.; Chen, E.; Yang, L.; Li, S.; Li, Y.; Zhang, L. “Two birds with one stone” strategy for the lung cancer therapy with bioinspired AIE aggregates. *J. Nanobiotechnol.* **2023**, *21*, 49. [[CrossRef](#)]
34. Jiang, W.; Cheng, C.; Qiu, X.; Chen, L.; Guo, X.; Luo, Y.; Wang, J.; Wang, J.; Xie, Z.; Li, P.; et al. Peptide Supramolecular Assembly-Instructed In Situ Self-Aggregation for Stratified Targeting Sonodynamic Therapy Enhancement of AIE Luminogens. *Adv. Sci.* **2023**, *10*, 2204989. [[CrossRef](#)]
35. Wu, M.-Y.; Chen, L.; Chen, Q.; Hu, R.; Xu, X.; Wang, Y.; Li, J.; Feng, S.; Dong, C.; Zhang, X.-L.; et al. Engineered Phage with Aggregation-Induced Emission Photosensitizer in Cocktail Therapy against Sepsis. *Adv. Mater.* **2023**, *35*, 2208578. [[CrossRef](#)] [[PubMed](#)]
36. Zhang, T.; Chen, X.; Yuan, C.; Pang, X.; Shanguan, P.; Liu, Y.; Han, L.; Sun, J.; Lam, J.W.Y.; Liu, Y.; et al. Near-Infrared Aggregation-Induced Emission Luminogens for In Vivo Theranostics of Alzheimer’s Disease. *Angew. Chem. Int. Ed.* **2023**, *62*, e202211550. [[CrossRef](#)]
37. Liu, S.; Li, Y.; Kwok, R.T.K.; Lam, J.W.Y.; Tang, B.Z. Structural and process controls of AIEgens for NIR-II theranostics. *Chem. Sci.* **2020**, *12*, 3427–3436. [[CrossRef](#)]
38. Liu, Y.; Li, Y.; Koo, S.; Sun, Y.; Liu, Y.; Liu, X.; Pan, Y.; Zhang, Z.; Du, M.; Lu, S.; et al. Versatile Types of Inorganic/Organic NIR-IIa/IIb Fluorophores: From Strategic Design toward Molecular Imaging and Theranostics. *Chem. Rev.* **2022**, *122*, 209–268. [[CrossRef](#)]
39. Xu, C.; Pu, K. Second near-infrared photothermal materials for combinational nanotheranostics. *Chem. Soc. Rev.* **2021**, *50*, 1111–1137. [[CrossRef](#)] [[PubMed](#)]
40. Shao, A.; Xie, Y.; Zhu, S.; Guo, Z.; Zhu, S.; Guo, J.; Shi, P.; James, T.D.; Tian, H.; Zhu, W.H. Far-Red and Near-IR AIE-Active Fluorescent Organic Nanoprobes with Enhanced Tumor-Targeting Efficacy: Shape-Specific Effects. *Angew. Chem. Int. Ed. Engl.* **2015**, *54*, 7275–7280. [[CrossRef](#)]
41. Gu, X.; Yao, J.; Zhang, G.; Zhang, C.; Yan, Y.; Zhao, Y.; Zhang, D. New electron-donor/acceptor-substituted tetraphenylethylenes: Aggregation-induced emission with tunable emission color and optical-waveguide behavior. *Chem. Asian J.* **2013**, *8*, 2362–2369. [[CrossRef](#)] [[PubMed](#)]
42. Xu, W.; Lee, M.M.S.; Zhang, Z.; Sung, H.H.Y.; Williams, I.D.; Kwok, R.T.K.; Lam, J.W.Y.; Wang, D.; Tang, B.Z. Facile synthesis of AIEgens with wide color tunability for cellular imaging and therapy. *Chem. Sci.* **2019**, *10*, 3494–3501. [[CrossRef](#)]
43. Ajayaghosh, A. Donor–acceptor type low band gap polymers: Polysquaraines and related systems. *Chem. Soc. Rev.* **2003**, *32*, 181–191. [[CrossRef](#)] [[PubMed](#)]

44. Zhou, T.; Jia, T.; Kang, B.; Li, F.; Fahlman, M.; Wang, Y. Nitrile-substituted QA derivatives: New acceptor materials for solution-processable organic bulk heterojunction solar cells. *Adv. Energy Mater.* **2011**, *1*, 431–439. [[CrossRef](#)]
45. Kolb, H.C.; Finn, M.G.; Sharpless, K.B. Click chemistry: Diverse chemical function from a few good reactions. *Angew. Chem. Int. Ed.* **2001**, *40*, 2004–2021. [[CrossRef](#)]
46. Michinobu, T.; Diederich, F. The [2+2] Cycloaddition-Retroelectrocyclization (CA-RE) Click Reaction: Facile Access to Molecular and Polymeric Push-Pull Chromophores. *Angew. Chem. Int. Ed.* **2018**, *57*, 3552–3577. [[CrossRef](#)] [[PubMed](#)]
47. Shoji, T.; Ito, S. Azulene-based donor-acceptor systems: Synthesis, optical, and electrochemical properties. *Chem.-Eur. J.* **2017**, *23*, 16696–16709. [[CrossRef](#)]
48. Bruce, M.I.; Rodgers, J.R.; Snow, M.R.; Swincer, A.G. Cyclopentadienyl-ruthenium and -osmium chemistry. Cleavage of tetracyanoethylene under mild conditions: X-ray crystal structures of [Ru( $\eta$ -3-C(CN)<sub>2</sub>CPhCC(CN)<sub>2</sub>)(PPh<sub>3</sub>)( $\eta$ -C<sub>5</sub>H<sub>5</sub>)] and [Ru(C[C(CN)<sub>2</sub>]CPhC(CN)<sub>2</sub>)-(CNBut)(PPh<sub>3</sub>)( $\eta$ -C<sub>5</sub>H<sub>5</sub>)]. *J. Chem. Soc. Chem Commun.* **1981**, *6*, 271–272. [[CrossRef](#)]
49. Cai, C.; Liakatas, I.; Wong, M.-S.; Bösch, M.; Bosshard, C.; Günter, P.; Concilio, S.; Tirelli, N.; Suter, U.W. Donor–Acceptor-Substituted Phenylethynyl Bithiophenes: Highly Efficient and Stable Nonlinear Optical Chromophores. *Org. Lett.* **1999**, *1*, 1847–1849. [[CrossRef](#)]
50. Wu, X.; Wu, J.; Liu, Y.; Jen, A.K.Y. Highly Efficient, Thermally and Chemically Stable Second Order Nonlinear Optical Chromophores Containing a 2-Phenyl-tetracyanobutadienyl Acceptor. *J. Am. Chem. Soc.* **1999**, *121*, 472–473. [[CrossRef](#)]
51. Michinobu, T.; Boudon, C.; Gisselbrecht, J.P.; Seiler, P.; Frank, B.; Moonen, N.N.; Gross, M.; Diederich, F. Donor-substituted 1,1,4,4-tetracyanobutadienes (TCBDS): New chromophores with efficient intramolecular charge-transfer interactions by atom-economic synthesis. *Chem. Eur. J.* **2006**, *12*, 1889–1905. [[CrossRef](#)]
52. Michinobu, T.; May, J.C.; Lim, J.H.; Boudon, C.; Gisselbrecht, J.-P.; Seiler, P.; Gross, M.; Biaggio, I.; Diederich, F. A new class of organic donor–acceptor molecules with large third-order optical nonlinearities. *Chem. Commun.* **2005**, *6*, 737–739. [[CrossRef](#)] [[PubMed](#)]
53. Kivala, M.; Boudon, C.; Gisselbrecht, J.P.; Enko, B.; Seiler, P.; Müller, I.B.; Langer, N.; Jarowski, P.D.; Gescheidt, G.; Diederich, F. Organic super-acceptors with efficient intramolecular charge-transfer interactions by [2+2] cycloadditions of TCNE, TCNQ, and F4-TCNQ to donor-substituted cyanoalkynes. *Chem. Eur. J.* **2009**, *15*, 4111–4123. [[CrossRef](#)] [[PubMed](#)]
54. Kivala, M.; Boudon, C.; Gisselbrecht, J.-P.; Seiler, P.; Gross, M.; Diederich, F. A novel reaction of 7,7,8,8-tetracyanoquinodimethane (TCNQ): Charge-transfer chromophores by [2 + 2] cycloaddition with alkynes. *Chem. Commun.* **2007**, *45*, 4731–4733. [[CrossRef](#)]
55. Reutenauer, P.; Kivala, M.; Jarowski, P.D.; Boudon, C.; Gisselbrecht, J.P.; Gross, M.; Diederich, F. New strong organic acceptors by cycloaddition of TCNE and TCNQ to donor-substituted cyanoalkynes. *Chem. Commun.* **2007**, *46*, 4898–4900. [[CrossRef](#)] [[PubMed](#)]
56. Patil, Y.; Misra, R. Diketopyrrolopyrrole-Based and Tetracyano-Bridged Small Molecules for Bulk Heterojunction Organic Solar Cells. *Chem.-Asian J.* **2018**, *13*, 220–229. [[CrossRef](#)] [[PubMed](#)]
57. Rout, Y.; Chauhan, V.; Misra, R. Synthesis and Characterization of Isoindigo-Based Push-Pull Chromophores. *J. Org. Chem.* **2020**, *85*, 4611–4618. [[CrossRef](#)] [[PubMed](#)]
58. Rao, P.S.; More, V.G.; Jangale, A.D.; Bhosale, S.V.; Bhosale, R.S.; Puyad, A.L.; Chen, J.-Y.; Li, J.-L.; Bhosale, S.V.; Gupta, A.; et al. A series of V-shaped small molecule non-fullerene electron acceptors for efficient bulk-heterojunction devices. *Dyes Pigm.* **2019**, *171*, 107677. [[CrossRef](#)]
59. Rao, P.S.; Puyad, A.L.; Bhosale, S.V.; Bhosale, S.V. Triphenylamine-merocyanine-based D1-A1- $\pi$ -A2/A3-D2 chromophore system: Synthesis, optoelectronic, and theoretical studies. *Int. J. Mol. Sci.* **2019**, *20*, 1621. [[CrossRef](#)]
60. Rout, Y.; Misra, R.; Singhal, R.; Biswas, S.; Sharma, G.D. Phenothiazine-based small-molecule organic solar cells with power conversion efficiency over 7% and open circuit voltage of about 1.0 V using solvent vapor annealing. *Phys. Chem. Chem. Phys.* **2018**, *20*, 6321–6329. [[CrossRef](#)]
61. Srinivasa Rao, P.; Gupta, A.; Bhosale, S.V.; Bilic, A.; Xiang, W.; Evans, R.A.; Bhosale, S.V. Donor-acceptor-acceptor-based non-fullerene acceptors comprising terminal chromen-2-one functionality for efficient bulk-heterojunction devices. *Dyes Pigm.* **2017**, *146*, 502–511. [[CrossRef](#)]
62. Gautam, P.; Misra, R.; Sharma, G.D. Dicyanoquinodimethane-substituted benzothiadiazole for efficient small-molecule solar cells. *Phys. Chem. Chem. Phys.* **2016**, *18*, 7235–7241. [[CrossRef](#)] [[PubMed](#)]
63. He, W.; Washino, Y.; Murata, K.; Nozaki, N.; Matsumoto, H.; Michinobu, T. [2+2] Cycloaddition-retroelectrocyclization reactivity and thin film transistor performances of carbazole-based platinum polyynic polymers. *Mater. Chem. Phys.* **2022**, *281*, 125861. [[CrossRef](#)]
64. Leliège, A.; Blanchard, P.; Rousseau, T.; Roncali, J. Triphenylamine/Tetracyanobutadiene-Based D-A-D  $\pi$ -Conjugated Systems as Molecular Donors for Organic Solar Cells. *Org. Lett.* **2011**, *13*, 3098–3101. [[CrossRef](#)] [[PubMed](#)]
65. Raheem, A.A.; Murugan, P.; Shanmugam, R.; Praveen, C. Azulene Bridged  $\pi$ -Distorted Chromophores: The Influence of Structural Symmetry on Optoelectrochemical and Photovoltaic Parameters. *ChemPlusChem* **2021**, *86*, 1451–1460. [[CrossRef](#)] [[PubMed](#)]
66. Philippe, C.; Melan, J.; Barsella, A.; Vives, T.; Leroux, Y.R.; Robin-Le Guen, F.; Lemiegre, L.; Jacquemin, D.; Gauthier, S.; Trolez, Y. A comprehensive study of tetracyanobutadiene push-pull chromophores derived from  $\gamma$ -pyranilidene. *Tetrahedron Chem.* **2023**, *5*, 100036. [[CrossRef](#)]
67. Pokladek, Z.; Ripoche, N.; Betou, M.; Trolez, Y.; Mongin, O.; Olesiak-Banska, J.; Matczyszyn, K.; Samoc, M.; Humphrey, M.G.; Blanchard-Desce, M.; et al. Linear Optical and Third-Order Nonlinear Optical Properties of Some Fluorenyl- and Triarylamine-Containing Tetracyanobutadiene Derivatives. *Chem. Eur. J.* **2016**, *22*, 10155–10167. [[CrossRef](#)]

68. Ripoche, N.; Betou, M.; Philippe, C.; Trolez, Y.; Mongin, O.; Dudek, M.; Pokladek, Z.; Matczyszyn, K.; Samoc, M.; Sahnoune, H.; et al. Two-photon absorption properties of multipolar triarylamino/tosylamido 1,1,4,4-tetracyanobutadienes. *Phys. Chem. Chem. Phys.* **2021**, *23*, 22283–22297. [[CrossRef](#)]
69. Mammadova, F.; Inyurt, F.C.; Barsella, A.; Dengiz, C. Cyano-rich donor-acceptor-donor-type NLOphores containing dialkylated triazene and aniline groups. *Dyes Pigm.* **2023**, *209*, 110894. [[CrossRef](#)]
70. Zhao, P.; Wang, D.; Gao, H.; Zhang, J.; Xing, Y.; Yang, Z.; Cao, H.; He, W. Third-order nonlinear optical properties of the “clicked” closed-ring spiropyrans. *Dyes Pigm.* **2019**, *162*, 451–458. [[CrossRef](#)]
71. Miao, Z.; Han, H.; Wang, D.; Gao, H.; Gu, J.; Hu, H. Nonlinear optical and energy-level modulation of organic alkynes by click chemistry. *Tetrahedron* **2016**, *72*, 4039–4046. [[CrossRef](#)]
72. Yang, L.; Li, L.; Gao, H.; Wang, D.; Yang, Z.; Cao, H.; He, W. Photoacoustic effect of azo derivatives modified by click reagents and parceled by liposomes. *Dyes Pigm.* **2020**, *172*, 107822. [[CrossRef](#)]
73. Gao, H.; Zhao, Z.; Liu, W.; Wang, D.; He, W.; Cao, H.; Yang, Z. Novel application of NIR photoacoustic absorbing dyes in thermosensitive micelles. *Dyes Pigm.* **2019**, *164*, 319–326. [[CrossRef](#)]
74. Zhao, Z.; Wang, D.; Gao, H.; Yang, Z.; Cao, H.; He, W. Photoacoustic effect of near-infrared absorbing fullerene derivatives with click moieties. *Dyes Pigm.* **2019**, *164*, 182–187. [[CrossRef](#)]
75. Li, L.; Wang, D.; Wang, L.; Ramella, D.; Wang, H.; Gao, H.; Zhang, J.; Xing, Y.; Li, B.; Yang, Z.; et al. The photoacoustic effect of near-infrared absorbing porphyrin derivatives prepared via click chemistry. *Dyes Pigm.* **2018**, *148*, 501–507. [[CrossRef](#)]
76. Xu, A.-P.; Han, H.-H.; Lu, J.; Yang, P.-P.; Gao, Y.-J.; An, H.-W.; Zhannng, D.; Li, L.-Z.; Zhang, J.-P.; Wang, D.; et al. Charge transfer NIR dyes for improved photoacoustic effect. *Dyes Pigm.* **2016**, *125*, 392–398. [[CrossRef](#)]
77. Shi, H.; Gu, R.; Xu, W.; Huang, H.; Xue, L.; Wang, W.; Zhang, Y.; Si, W.; Dong, X. Near-Infrared Light-Harvesting Fullerene-Based Nanoparticles for Promoted Synergetic Tumor Phototheranostics. *ACS Appl. Mater. Interfaces* **2019**, *11*, 44970–44977. [[CrossRef](#)]
78. Tang, B.; Qin, A.; Han, P.; Zhang, G.; Xu, H. Preparation of Organic Near-Infrared Photothermal Materials and Its Application. CN115,043,756, 13 September 2022.
79. Bhusanur, D.I.; Nadimetla, D.N.; Harmalkar, S.S.; Bhosale, R.S.; Puyad, A.L.; Wagalgave, S.M.; Bhosale, S.V.; Bhosale, S.V. Synthesis, crystal structure and supramolecular self-assembly of tetraphenylethylene subunit appended isoindigo derivatives. *J. Mol. Struct.* **2022**, *1255*, 132452. [[CrossRef](#)]
80. Philippe, C.; Coste, M.; Bretonniere, Y.; Lemiegre, L.; Ulrich, S.; Trolez, Y. Quadruple Functionalization of a Tetraphenylethylene Aromatic Scaffold with Ynamides or Tetracyanobutadienes: Synthesis and Optical Properties. *Eur. J. Org. Chem.* **2022**, *2022*, e202200049. [[CrossRef](#)]
81. Zhao, Z.; Chen, C.; Wu, W.; Wang, F.; Du, L.; Zhang, X.; Xiong, Y.; He, X.; Cai, Y.; Kwok, R.T.K.; et al. Highly efficient photothermal nanoagent achieved by harvesting energy via excited-state intramolecular motion within nanoparticles. *Nat. Commun.* **2019**, *10*, 768. [[CrossRef](#)]
82. Fesser, P.; Iacovita, C.; Wäckerlin, C.; Vijayaraghavan, S.; Ballav, N.; Howes, K.; Gisselbrecht, J.-P.; Crobu, M.; Boudon, C.; Stöhr, M.; et al. Visualizing the Product of a Formal Cycloaddition of 7,7,8,8-Tetracyano-p-quinodimethane (TCNQ) to an Acetylene-Appended Porphyrin by Scanning Tunneling Microscopy on Au(111). *Chem. Eur. J.* **2011**, *17*, 5246–5250. [[CrossRef](#)]
83. Liu, X.; Wang, D.; Gao, H.; Yang, Z.; Xing, Y.; Cao, H.; He, W.; Wang, H.; Gu, J.; Hu, H. Nonlinear optical properties of symmetrical and asymmetrical porphyrin derivatives with click chemistry modification. *Dyes Pigm.* **2016**, *134*, 155–163. [[CrossRef](#)]
84. Wang, D.; Zhang, W.; Xing, Y.; Gao, H.; Wang, X.; Zhao, Y.; Yang, H. Energy-level modulation of organic alkynes by click chemistry. *Tetrahedron* **2013**, *69*, 895–901. [[CrossRef](#)]
85. Zhao, Y.; Liu, X.; Li, Q.; Guo, Z.; He, Z.; Zhang, H.; Ma, C.; Gao, J.; Zhao, Y.; Wang, D. Preparation of Polyphenylene Ring Derivative Dyes with Wide Wave Absorption Properties and Their Performance Study. *Molecules* **2022**, *27*, 5551. [[CrossRef](#)] [[PubMed](#)]
86. Zhao, Y.; Liu, X.; Zhao, X.; Li, Q.; Zhao, Y.; Guo, Z.; He, Z.; Zhang, H.; Gao, J.; Miao, Z. Preparation of symmetrical and asymmetrical multi-phenylene ring nonlinear optical materials with click chemical modifications and their properties. *Tetrahedron* **2022**, *127*, 132992. [[CrossRef](#)]
87. Dar, A.H.; Gowri, V.; Gopal, A.; Muthukrishnan, A.; Bajaj, A.; Sartaliya, S.; Selim, A.; Ali, E.M.; Jayamurugan, G. Designing of Push-Pull Chromophores with Tunable Electronic and Luminescent Properties Using Urea as the Electron Donor. *J. Org. Chem.* **2019**, *84*, 8941–8947. [[CrossRef](#)] [[PubMed](#)]
88. Simon Marques, P.; Castan, J.M.A.; Raul, B.A.L.; Londi, G.; Ramirez, I.; Pshenichnikov, M.S.; Beljonne, D.; Walzer, K.; Blais, M.; Allain, M.; et al. Triphenylamine/Tetracyanobutadiene-Based  $\pi$ -Conjugated Push-Pull Molecules End-Capped with Arene Platforms: Synthesis, Photophysics, and Photovoltaic Response. *Chem.-Eur. J.* **2020**, *26*, 16422–16433. [[CrossRef](#)]
89. Philippe, C.; Bui, A.T.; Beau, M.; Bloux, H.; Riobe, F.; Mongin, O.; Roisnel, T.; Cordier, M.; Paul, F.; Lemiegre, L.; et al. Synthesis and Photophysical Properties of 1,1,4,4-Tetracyanobutadienes Derived from Ynamides Bearing Fluorophores. *Chem.-Eur. J.* **2022**, *28*, e202200025. [[CrossRef](#)]
90. Parr, R.G.; Yang, W. *Density-Functional Theory of Atoms and Molecules*; Clarendon Press: Oxford, UK, 1989.
91. Runge, E.; Gross, E.K.U. Density-functional theory for time-dependent systems. *Phys. Rev. Lett.* **1984**, *52*, 997–1000. [[CrossRef](#)]
92. Stratmann, R.E.; Scuseria, G.E.; Frisch, M.J. An efficient implementation of time-dependent density-functional theory for the calculation of excitation energies of large molecules. *J. Chem. Phys.* **1998**, *109*, 8218–8224. [[CrossRef](#)]

93. Trickey, S.B. Recent Advances in Density Functional Methods—Part I by Delano P. Chong. *Int. J. Quantum Chem.* **1999**, *72*, 155–156. [[CrossRef](#)]
94. Zhao, Y.; Truhlar, D.G. Density Functionals with Broad Applicability in Chemistry. *Acc. Chem. Res.* **2008**, *41*, 157–167. [[CrossRef](#)]
95. Yanai, T.; Tew, D.P.; Handy, N.C. A new hybrid exchange-correlation functional using the Coulomb-attenuating method (CAM-B3LYP). *Chem. Phys. Lett.* **2004**, *393*, 51–57. [[CrossRef](#)]
96. Adamo, C.; Jacquemin, D. The calculations of excited-state properties with Time-Dependent Density Functional Theory. *Chem. Soc. Rev.* **2013**, *42*, 845–856. [[CrossRef](#)]
97. Martin, R.L. Natural transition orbitals. *J. Chem. Phys.* **2003**, *118*, 4775–4777. [[CrossRef](#)]
98. Etienne, T.; Assfeld, X.; Monari, A. Toward a Quantitative Assessment of Electronic Transitions' Charge-Transfer Character. *J. Chem. Theory Comput.* **2014**, *10*, 3896–3905. [[CrossRef](#)] [[PubMed](#)]
99. Etienne, T.; Assfeld, X.; Monari, A. New Insight into the Topology of Excited States through Detachment/Attachment Density Matrices-Based Centroids of Charge. *J. Chem. Theory Comput.* **2014**, *10*, 3906–3914. [[CrossRef](#)] [[PubMed](#)]
100. Han, P.; Zhang, G.; Xu, H.; Hu, R.; Qin, A.; Tang, B.Z. Organic near infrared photothermal materials with temperatures up to 450°C constructed by cycloaddition-retroelectrocyclization click reaction. *ChemRxiv* **2022**, 1–32. [[CrossRef](#)]
101. Bancziger, S.D.; Clendening, R.A.; Oxley, B.M.; Ren, T. Spectroelectrochemical and Computational Analysis of a Series of Cycloaddition-Retroelectrocyclization-Derived Donor-Acceptor Chromophores. *J. Phys. Chem. B* **2020**, *124*, 11901–11909. [[CrossRef](#)]
102. Gautam, P.; Maragani, R.; Misra, R. Tuning the HOMO-LUMO gap of donor-substituted benzothiazoles. *Tetrahedron Lett.* **2014**, *55*, 6827–6830. [[CrossRef](#)]
103. Jin, Z.; Wang, D.; Wang, X.; Liang, P.; Mi, Y.; Yang, H. Efficient modification of pyrene-derivative featuring third-order nonlinear optics via the click post-functionalization. *Tetrahedron Lett.* **2013**, *54*, 4859–4864. [[CrossRef](#)]
104. Liang, P.; Du, Z.; Wang, D.; Yang, Z.; Sheng, H.; Liang, S.; Cao, H.; He, W.; Yang, H. Optoelectronic and Self-assembly Properties of Porphyrin Derivatives with Click Chemistry Modification. *ChemPhysChem* **2014**, *15*, 3523–3529. [[CrossRef](#)]
105. Mi, Y.; Liang, P.; Jin, Z.; Wang, D.; Yang, Z. Synthesis and Third-Order Nonlinear Optical Properties of Triphenylene Derivatives Modified by Click Chemistry. *ChemPhysChem* **2013**, *14*, 4102–4108. [[CrossRef](#)] [[PubMed](#)]
106. Misra, R.; Gautam, P. Tuning of the HOMO-LUMO gap of donor-substituted symmetrical and unsymmetrical benzothiadiazoles. *Org. Biomol. Chem.* **2014**, *12*, 5448–5457. [[CrossRef](#)] [[PubMed](#)]
107. Rout, Y.; Gautam, P.; Misra, R. Unsymmetrical and Symmetrical Push-Pull Phenothiazines. *J. Org. Chem.* **2017**, *82*, 6840–6845. [[CrossRef](#)] [[PubMed](#)]
108. Rout, Y.; Jang, Y.; Gobeze, H.B.; Misra, R.; D'Souza, F. Conversion of Large-Bandgap Triphenylamine-Benzothiadiazole to Low-Bandgap, Wide-Band Capturing Donor-Acceptor Systems by Tetracyanobutadiene and/or Dicyanoquinodimethane Insertion for Ultrafast Charge Separation. *J. Phys. Chem. C* **2019**, *123*, 23382–23389. [[CrossRef](#)]
109. Sharma, R.; Maragani, R.; Misra, R. C<sub>3</sub>-Symmetric star shaped donor-acceptor truxenes: Synthesis and photophysical, electrochemical and computational studies. *New J. Chem.* **2018**, *42*, 882–890. [[CrossRef](#)]
110. Sharma, R.; Thomas, M.B.; Misra, R.; D'Souza, F. Strong Ground- and Excited-State Charge Transfer in C<sub>3</sub>-Symmetric Truxene-Derived Phenothiazine-Tetracyanobutadiene and Expanded Conjugates. *Angew. Chem. Int. Ed.* **2019**, *58*, 4350–4355. [[CrossRef](#)]
111. Zhang, W.-S.; Wang, D.; Cao, H.; Yang, H. Energy level tunable pre-click functionalization of [60]fullerene for nonlinear optics. *Tetrahedron* **2014**, *70*, 573–577. [[CrossRef](#)]
112. Zhang, Z.; Gou, G.; Wan, J.; Li, H.; Wang, M.; Li, L. Synthesis, Structure, and Significant Energy Gap Modulation of Symmetrical Silafluorene-Cored Tetracyanobutadiene and Tetracyanoquinodimethane Derivatives. *J. Org. Chem.* **2022**, *87*, 2470–2479. [[CrossRef](#)]
113. Coulson, D.R.; Satek, L.C.; Grim, S.O. Tetrakis(Triphenylphosphine)Palladium(0). In *Inorganic Syntheses*; John Wiley & Sons, Inc.: Hoboken, NJ, USA, 1990; Volume 28, pp. 107–109.
114. Meier, H.; Muehling, B.; Kolshorn, H. Red- and blue-shifts in oligo(1,4-phenyleneethynylene)s having terminal donor-acceptor substitutions. *Eur. J. Org. Chem.* **2004**, *5*, 1033–1042. [[CrossRef](#)]
115. Makula, P.; Pacia, M.; Macyk, W. How to correctly determine the band gap energy of modified semiconductor photocatalysts based on UV–Vis spectra. *J. Phys. Lett.* **2018**, *9*, 6814–6817. [[CrossRef](#)] [[PubMed](#)]
116. COMSOL Multiphysics, V. 6.0. COMSOL AB: Stockholm, Sweden. Available online: [www.comsol.com](http://www.comsol.com) (accessed on 1 January 2023).
117. Frisch, M.J.; Trucks, G.W.; Schlegel, H.B.; Scuseria, G.E.; Robb, M.A.; Cheeseman, J.R.; Scalmani, G.; Barone, V.; Mennucci, B.; Petersson, G.A.; et al. *Gaussian 09 Rev. D.01*; Gaussian, Inc.: Wallington, CT, USA, 2016.
118. Tomasi, J.; Mennucci, B.; Cammi, R. Quantum Mechanical Continuum Solvation Models. *Chem. Rev.* **2005**, *105*, 2999–3093. [[CrossRef](#)] [[PubMed](#)]

**Disclaimer/Publisher's Note:** The statements, opinions and data contained in all publications are solely those of the individual author(s) and contributor(s) and not of MDPI and/or the editor(s). MDPI and/or the editor(s) disclaim responsibility for any injury to people or property resulting from any ideas, methods, instructions or products referred to in the content.